Mathematical Problems in Engineering

Mathematical Modeling and Analysis of Soft Computing in Smart Buildings

Lead Guest Editor: Federico Divina
Guest Editors: Miguel G. Torres, Francisco C. De la O., and Enrico Blanzieri

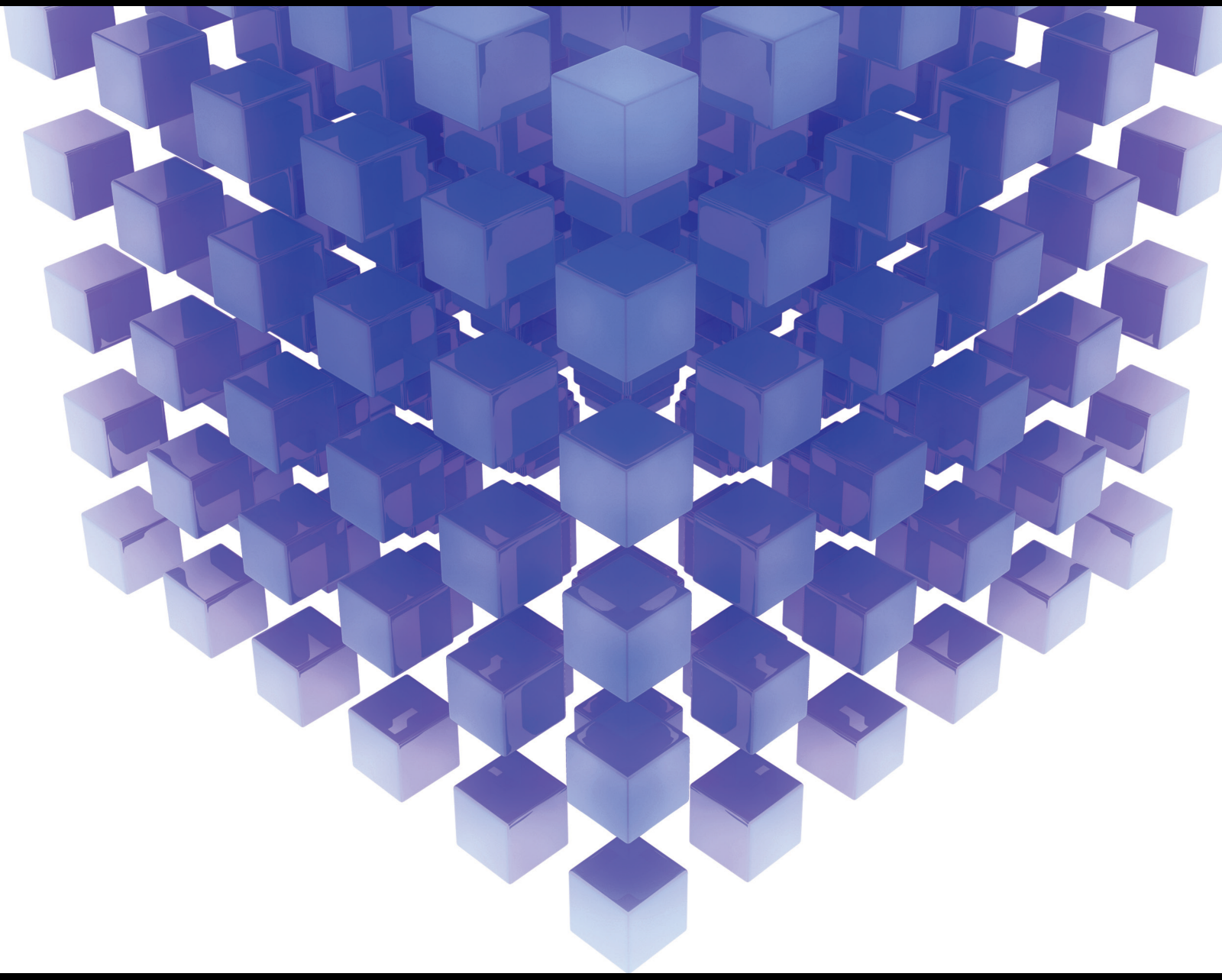

Mathematical Modeling and Analysis of Soft Computing in Smart Buildings

Mathematical Problems in Engineering

Mathematical Modeling and Analysis of Soft Computing in Smart Buildings

Lead Guest Editor: Federico Divina
Guest Editors: Miguel G. Torres, Francisco C. De la O., and Enrico Blanzieri

Contents

Dynamic Hybrid Multiple Attribute Decision-Making Problem Based on Reference Point Adaptation
Wei-Min Ma, Hui Zhang, Bing-Zhen Sun, Neng-Li Wang, and Hai-Yan Zhao
Research Article (8 pages), Article ID 9470172, Volume 2019 (2019)

Airflow Patterns around Obstacles with Large-Span Shallow Shell Roof: Wind Tunnel Measurements and Direct Simulation
Hongying Jia, Huixue Dang, Qianying Ma, and Jun-Hai Zhao
Research Article (11 pages), Article ID 9619282, Volume 2019 (2019)

Dynamic Network Planning of Underground Logistics System on Uncertainty Graph
YiHua Zhong, ShiMing Luo, Min Bao, and XiaoDie Lv
Research Article (13 pages), Article ID 1979275, Volume 2019 (2019)

Spatial Reasoning Based on 3D-ICSRM Model
Yongshan Liu, Xiang Gong, and Dehan Kong
Research Article (9 pages), Article ID 2892545, Volume 2019 (2019)

Hindawi
Mathematical Problems in Engineering
Volume 2019, Article ID 9470172, 8 pages
https://doi.org/10.1155/2019/9470172

Research Article

Dynamic Hybrid Multiple Attribute Decision-Making Problem Based on Reference Point Adaptation

Wei-Min Ma,[1] Hui Zhang,[1] Bing-Zhen Sun,[2] Neng-Li Wang,[3] and Hai-Yan Zhao[4]

[1]*School of Economics and Management, Tongji University, Shanghai 200092, China*
[2]*School of Economics and Management, Xidian University, Xi'an, Shaanxi 710071, China*
[3]*The Center for Pediatric Liver Diseases, Children's Hospital of Fudan University, Shanghai 201102, China*
[4]*School of Management, Shanghai University of Engineering Science, Shanghai 201620, China*

Correspondence should be addressed to Hui Zhang; graduation2018@sina.com

Received 2 June 2019; Revised 20 August 2019; Accepted 3 October 2019; Published 29 November 2019

Guest Editor: Federico Divina

Individuals' decision-making depends on reference points in prospect theory. This research considers the bounded rationality of decision makers and constructs a dynamic hybrid multiple attribute decision-making (DHMADM) model. Unlike existing models, the DHMADM model focuses on dynamic reference point, which has been proven in prospect theory. This research presents the effects of reference point adaptation on decision-making through model calculation. The optimal choice of decision makers changed with the change of the reference point in the DHMADM model. By experiment, we found that the DHMADM model considering reference point adaptation can more accurately express the final choice of decision makers than models only considering the static reference point.

1. Introduction

We live in a rapidly developing world, and human cognition has limitations and subjectivity. Consequently, individuals experience difficulty in making risky decisions. Multiple attribute decision-making (MADM) is aimed at choosing the best option from a set of possible options [1]. The consideration of multiple attributes helps decision makers (DMs) in choosing a suitable candidate from a number of alternatives [2]. Alternatives, attributes, and weights of these attributes are the main parts of MADM [3]. The weight of an attribute is an important factor in MADM problems [4]. Each alternative has quantitative and qualitative attributes [5]. MADM is widely applied in social and economic areas [6–8].

The world is constantly changing. An increasing number of studies focus on dynamic MADM (DMADM) problems. The core of DMADM is the changeable decision information [9]. The attributes of alternatives [10], attribute weights [11, 12], and attribute values [13] also change as time changes. Xu [13] found that DMADM problems with attribute weights and values occur at different periods. He and Teng [14] investigated DMADM problems in which the attribute values are provided by DMs at different periods. Shen et al. [15] constructed a DMADM model with the weights of attributes in multiple stages and analyzed the competence of private enterprises. Ai and Yang [16] investigated DMADM problems with dynamic attribute values in the form of two-tuple linguistic information. Liu [17] presented a method to solve two-tuple linguistic DMADM problems with entropy weights. Su et al. [18] investigated DMADM problems with attribute values in the form of intuitionistic fuzzy numbers, which are provided by multiple DMs in different periods.

However, the aforementioned studies are based on rationality. Individuals are sometimes irrational [19], and psychology plays an important role in decision-making [20]. Certain studies on MADM are based on bounded rationality. The main theory based on bounded rationality is prospect theory, which is used to model and interpret decision-making in stock trading [21]. Prospect theory is useful in solving MADM problems. Fan et al. [22] proposed a method

with different formats of attribute aspirations to solve MADM problems. Peng et al. [23] proposed a method to solve random fuzzy MADM problems with fuzzy and unknown probability and attribute values on the basis of prospect theory. Li and Chen [24] extended the TOPSIS method for group decision-making on the basis of prospect theory. Liu and Liu [25] proposed a method based on reference points in prospect theory to solve MADM problems with linguistic attributes. Li and Zhang [26] introduced a useful method to solve DMADM problems with three-parameter interval gray numbers on the basis of prospect theory. Zhu et al. [27] considered multiple reference points in MADM problems with the interval numbers of attribute values. Dai et al. [28] introduced a method that considered dynamic information to solve MADM problems with attribute values, which are triangular fuzzy numbers. Liu et al. [29] proposed an MADM method based on prospect theory to solve problems with uncertain linguistic attribute values.

Existing studies have made significant contributions to address MADM problems. When prospect theory is applied to solve MADM problems, reference points are regarded as static. However, reference points have been proven to be changing in the research of reference points in prospect theory [30–34]. Static reference points are unable to reflect the psychological changes of DMs. Hence, the main idea of this paper is to construct a dynamic hybrid multiple attribute decision-making (DHMADM) model on the basis of reference point adaptation. In this model, the attributes and reference points are described in real numbers, interval numbers, and linguistic variables. After the model was established, an experiment was conducted to test the practicality and effectiveness of the model. We find that the optimal choice of DMs changed with the adaptation of the reference point. Furthermore, compared with the hybrid multiattribute decision-making (HMADM) model considering only static reference point, the DHMADM model considering dynamic reference point can more accurately express the final decision-making of the DMs.

The innovations of this work are as follows. First, this research is the application of the dynamic reference point in prospect theory to HMADM problems. The DHMADM model is established on the basis of reference point adaption. Such approach can effectively reflect the real psychological changes of DMs in the decision-making process. The model can also shed light on the combination of the principle of prospect theory and MADM problems. Second, the calculation process of the DHMADM model in this work shows how reference point adaptation influences the decision results of DMs, and it further enriches the existing conclusions of prospect theory.

2. Prospect Theory

Prospect theory is a descriptive theory based on bounded rationality. The manner by which individuals evaluate gains and losses depends on a reference point [35]. The result is seen as a gain when it is above the reference point and a loss when it is below it. Individuals are inclined toward risk aversion in the gain domain. By contrast, individuals are inclined toward risk seeking in the loss domain. The value function model is as follows:

$$V(x) = \begin{cases} x^{a}, & x \geq 0, \\ -\lambda(-x)^{\beta}, & x < 0, \end{cases} \tag{1}$$

where x denotes the evaluation relative to the reference point. When x is greater than zero, the subjective evaluation relative to the reference point is seen as a gain; when x is equal to zero, it is consistent with the reference point; and when x is less than zero, it is seen as a loss. Parameters α and β represent the sensitivity coefficients of the gain and loss areas. The values of α and β are calculated by psychological experiments and $\alpha = \beta = 0.88$. Parameter λ represents the loss aversion coefficient and $\lambda = 2.25$ [36].

3. DHMADM Problems with Reference Point Adaptation

3.1. Reference Point Adaptation. DMs evaluate gains and losses on the basis of reference points and not absolute wealth. Generally, reference points are nonstatic. Reference point adaptation results in changes in evaluation values and decision-making [37]. In reference point adaptation, the shape of the value function is assumed to be constant and moves along the x-axis. In Figure 1, R_0 and R_1 are assumed to be the reference points of A and B, respectively. A and B see P_1 as a loss. Thereafter, B adapts its reference point to R_2 under the information effect [38]. B takes the same P_1 as a gain, and his risk attitude changes correspondingly. Furthermore, B's evaluation and decision-making may change accordingly.

3.2. Description of the Decision-Making Problems. In DHMADM problems with reference point adaptation, m alternatives $A = \{A_1, A_2, \ldots, A_m\}$ and n attributes $C = \{C_1, C_2, \ldots, C_n\}$ are assumed to exist, with $m \geq 2$ and $n \geq 2$. $X = [x_{ij}]_{m\times n}$ is the decision matrix, where x_{ij} denotes attribute j of alternative i. $W = \{w_1, w_2, \ldots, w_n\}$ is the attribute weight vector, with $1 \geq W_j \geq 0$ and $\sum_{j=1}^{n} W_j = 1$. $Q = \{Q_1, Q_2, \ldots, Q_n\}$ is the attribute expectation vector, with Q_j denoting DMs' expectations of attributes C_j, that is, $Q_j = \{q_j^1, q_j^2, \ldots, q_j^k\}$, where q_j^t represents DMs' expectations of attributes C_j in the tth period. Expectations can be used as reference points for DMs to judge losses and benefits [39]. If $q_j^t \geq x_{ij}$, then the evaluation values of alternatives A_i for attributes C_j are losses; otherwise, they are gains. $D(x_{ij}, q_j^t)$ is the distance between the actual situation and the reference point.

C^R, C^I, and C^L are the subsets of real numbers, interval numbers, and linguistic variables, respectively. $C^R = \{C_1, C_2, \ldots, C_j\}$; $C^I = \{C_{j+1}, C_{j+2}, \ldots, C_{j_2}\}$; and $C^L = \{C_{j_2+1}, C_{j_2+2}, \ldots, C_{j_3}\}$. J_1, J_2, and J_3 are the values of the real numbers, interval numbers, and linguistic variables, respectively. $J = J_1 \cup J_2 \cup J_3$ and $C = C^R \cup C^I \cup C^L$.

The real numbers, interval numbers, and linguistic variables are standardized according to different formulas using the previous method [40]. When attribute value

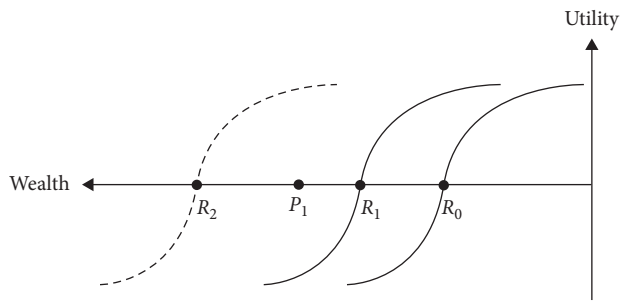

Figure 1: The potential role of reference point adaptation.

$C_j \in C^R$, the real numbers of the attribute values can be expressed as $x_{ij} = y^*_{ij}$. The real numbers of the corresponding reference points can be expressed as $q^t_j = z^{*t}_j$. When attribute value $C_j \in C^I$, the interval numbers of the attribute values can be expressed as $[x^L_{ij}, x^U_{ij}] = [y^{/L}_{ij}, y^{/U}_{ij}]$ and the corresponding reference points can then be expressed as $[q^{Lt}_j, q^{Ut}_j] = [z^{/Lt}_j, z^{/Ut}_j]$. When attribute value $C_j \in C^L$, the linguistic variables of the corresponding reference points can be expressed as follows:

$$s = \left(s^1, s^2, s^3\right) = \left(\max\left\{\frac{(f-1)}{T}, 0\right\}, \frac{f}{T}, \min\left\{\frac{(f+1)}{T}, 1\right\}\right), \tag{2}$$

where $T+1$ is the total number of phrases in a linguistic variable and $f+1$ refers to the geographical location of linguistic variables when describing attribute values and reference points.

The set of linguistic variables S can be inversely calculated with the method in [40] as follows:

$$S = \left\{s_f \,\middle|\, f = 0, 1, \ldots, \left(\frac{T}{2}\right) - 1, \frac{T}{2}, \left(\frac{T}{2}\right) + 1, \ldots, T\right\}, \tag{3}$$

where C_b is the set of attribute values for benefits, C_c is the set of attribute values for cost, and $C = C_b \cup C_c$.

4. Proposed Method

4.1. Data Processing Standardization. Three formats of reference points and attribute values need to be normalized to eliminate the influence of different physical dimensions on decision-making [41]. A reference point's vector $Q_j = \{q^1_j, q^2_j, \ldots, q^k_j\}$ is normalized into $Z^t_j = \{z^1_j, z^2_j, \ldots, z^k_j\}$, and decision matrix $X = [x_{ij}]_{m\times n}$ is normalized into $Y = [y_{ij}]_{m\times n}$ [41].

For $x_{ij} \in C^R$ and $q^t{}_j \in C^R$, the normalized formula for reference points is as follows:

$$z^{*t}_j = \begin{cases} \dfrac{q^t_j - x^-_j}{x^+_j - x^-_j}, & j \in Q_1 \cap Q_b, \\[2ex] \dfrac{x^+_j - q^t_j}{x^+_j - x^-_j}, & j \in Q_1 \cap Q_c. \end{cases} \tag{4}$$

The normalized formula for attribute values is as follows:

$$y^*_{ij} = \begin{cases} \dfrac{x^*_{ij} - x^-_j}{x^+_j - x^-_j}, & i \in M, j \in Q_1 \cap Q_b, \\[2ex] \dfrac{x^+_j - x^*_{ij}}{x^+_j - x^-_j}, & i \in M, j \in Q_1 \cap Q_c, \end{cases} \tag{5}$$

where

$$x^+_j = \max\left\{\max_{1\le i\le m}\left\{x^*_{ij}\right\}, q^t_j\right\}, \quad j \in Q_1, \tag{6}$$

$$x^-_j = \min\left\{\min_{1\le i\le m}\left\{x^*_{ij}\right\}, q^t_j\right\}, \quad j \in Q_1. \tag{7}$$

For $x_{ij} \in C^I$ and $q^t{}_j \in C^I$, the normalized formula for reference points is as follows:

$$\left[z^{/tL}_j, z^{/tU}_j\right] = \begin{cases} \left[\dfrac{q^{/tL}_j - x^{/L}_j}{x^{/U}_j - x^{/L}_j}, \dfrac{q^{/tU}_j - x^{/L}_j}{x^{/U}_j - x^{/L}_j}\right], & j \in Q_2 \cap Q_b, \\[2ex] \left[\dfrac{x^{/U}_j - q^{/tU}_j}{x^{/U}_j - x^{/L}_j}, \dfrac{x^{/U}_j - q^{/tL}_j}{x^{/U}_j - x^{/L}_j}\right], & j \in Q_2 \cap Q_c. \end{cases} \tag{8}$$

And the normalized formula for attribute values is as follows:

$$\left[y^{/L}_{ij}, y^{/U}_{ij}\right] = \begin{cases} \left[\dfrac{x^{/L}_{ij} - x^{/L}_j}{x^{/U}_j - x^{/L}_j}, \dfrac{x^{/U}_{ij} - x^{/L}_j}{x^{/U}_j - x^{/L}_j}\right], & i \in M, j \in Q_2 \cap Q_b, \\[2ex] \left[\dfrac{x^{/U}_{ij} - x^{/U}_j}{x^{/U}_j - x^{/L}_j}, \dfrac{x^{/U}_{ij} - x^{/L}_j}{x^{/U}_j - x^{/L}_j}\right], & i \in M, j \in Q_2 \cap Q_c, \end{cases} \tag{9}$$

where

$$x^{/U}_j = \max\left\{\max_{1\le i\le m}\left\{x^{/U}_{ij}\right\}, q^{/tU}_j\right\}, \quad j \in Q_2, \tag{10}$$

$$x^{/L}_j = \min\left\{\min_{1\le i\le m}\left\{x^{/L}_{ij}\right\}, q^{/tL}_j\right\}, \quad j \in Q_2. \tag{11}$$

For $x_{ij} \in C^L$ and $q^t{}_j \in C^L$, the normalized formula for reference points is as follows:

$$z^t_j = \begin{cases} q^t_j, & j \in Q_3 \cap Q_b, \\ \operatorname{neg}\left(q^t_j\right), & j \in Q_3 \cap Q_c. \end{cases} \tag{12}$$

And the normalized formula for attribute values is as follows:

$$y_{ij} = \begin{cases} x_{ij}, & i \in M, j \in Q_3 \cap Q_b, \\ \operatorname{neg}\left(x_{ij}\right), & i \in M, j \in Q_3 \cap Q_c. \end{cases} \tag{13}$$

According to equation (2), Z^t_j and y_{ij} can be converted into triangular fuzzy numbers $\hat{Z^t_j}$ and $\widehat{y_{ij}}$, respectively, for calculation, that is, $\hat{Z^t_j} = (Z^{1t}_j, Z^{2t}_j, Z^{3t}_j)$, $\widehat{y_{ij}} = (y^1_{ij}, y^2_{ij}, y^3_{ij})$.

4.2. Distance between Attribute Value and Reference Point. The distance between the attribute value and the reference point is expressed as follows:

$$D\left(y_{ij}, z_j^t\right) = \begin{cases} \left|y_{ij}^* - Z_j^{*t}\right|, & i \in M,\ j \in Q_1, \\ \sqrt{\frac{1}{2}\left[\left(y_{ij}^{/L} - Z_j^{/tL}\right)^2 + \left(y_{ij}^{/U} - Z_j^{tU}\right)^2\right]}, & i \in M,\ j \in Q_2, \\ \frac{1}{3}\left[\left(y_{ij}^1 - Z_j^{1t}\right)^2 + \left(y_{ij}^2 - Z_j^{2t}\right)^2 + \left(y_{ij}^3 - Z_j^{3t}\right)^2\right], & i \in M,\ j \in Q_3. \end{cases} \tag{14}$$

(1) For $x_{ij} \in C^R$, $D(z_{ij} - y_j^t) = z_{ij} - y_j^t$; if $z_{ij} \geq y_j^t$, then $D(z_{ij} - y_j^t)$ is a positive number; if $z_{ij} < y_j^t$, then $D(z_{ij} - y_j^t)$ is a negative number

(2) For $x_{ij} \in C^I$, if $M_1 \geq M_2$, then $D(z_{ij} - y_j^t)$ is a positive number; if $M_1 < M_2$, then $D(z_{ij} - y_j^t)$ is a negative number; $M_1 = (y_{ij}^L + y_{ij}^U)/2$ and $M_2 = (z_{ij}^L + z_{ij}^U)/2$

(3) For $x_{ij} \in C^L$, if $f > g$, then $s_f \succ s_g$, and $D(z_{ij} - y_j^t)$ is a positive number, and so on

4.3. Attribute Value. After the distance between the attribute value and the reference point is obtained, the value of each attribute is calculated by the value function of prospect theory. The gain and loss matrix relative to the reference point is obtained:

$$F = \left[F\left(y_{ij}^t\right)\right]_{m \times n \times k}. \tag{15}$$

Then, according to the values of sensitivity coefficients of the gain and loss areas and loss aversion coefficient, the corresponding prospect values are calculated according to equation (1):

$$V\left(F\left(y_{ij}\right)\right) = \begin{cases} \left(F\left(y_{ij}\right)\right)^{\alpha}, & y_{ij} \geq z_j^t, \\ -\lambda\left(F\left(y_{ij}\right)\right)^{\beta}, & y_{ij} < z_j^t. \end{cases} \tag{16}$$

4.4. Attribute Utility. Finally, the utility values of each alternative are calculated and compared according to the weights. The ranking of all alternatives will be determined according to the comprehensive prospects calculated by the following formula. The larger the value, the more likely the DMs will prefer the alternative. The smaller the value, the less likely the DMs will choose the alternative. The numerical value of the comprehensive prospect value may also be negative, indicating that the alternative does not meet the ideal criteria of DMs:

$$U(A_i) = \sum_{j=1}^{n} w_j V\left(F\left(y_{ij}\right)\right). \tag{17}$$

5. Case Study

An experiment on a hypothetical scenario involving a newly opened furniture store is carried out to illustrate the relationship between reference point adaptation and decision-making. At the same time, compare the HMADM model considering only static reference points with the DHMADM model considering dynamic reference points and test which model can more accurately express the DMs' final decision-making.

5.1. Experimental Design. The locations of furniture store directly affect sales, and thus, the most appropriate address must be chosen. The following four factors are considered in the selection of furniture store locations: geographical location C_1, annual rent C_2, decoration cost C_3, and transfer C_4. Geographical location includes the location of shops, the demand around them, and traffic conditions. Annual rent refers to the one-year rent paid by the user of a shop to the owner. Rent is high when the store is near large furniture markets. Decoration cost is regarded as the resources spent in the design and construction activities to make shops beautiful. Transfer means the possibility and acceptance time of other people in the process of transferring the right to use the store.

We present a hypothetical scenario for opening a new store because of business needs and interviewed a furniture brand manager on August 27, 2018. In the hypothetical scenario, the manager needs to select an appropriate store from $A1$, $A2$, and $A3$. The selection was given to the furniture store manager for further evaluation. These three alternatives use four attributes for description: geographical location, annual rent, decoration cost, and transfer. The geographical location and transfer are described as very good (VG), good (G), common (C), poor (P), and very poor (VP). The annual rent and decoration cost are described by real and interval numbers, respectively (Table 1).

Step 1: As in an experiment for a supplier selection problem, DMs themselves can provide the attribute weights [42]. The manager in the experiment was asked to assign weights to the four factors. The weight of a factor is great if it is important. However, the total weight of ownership should not be more than 1.

Step 2: After determining the weights of all factors, the manager was asked to express any expectations toward the four factors. This aspect was set as the first reference point of the manager.

Step 3: The manager was then asked to rank the three alternatives: A1, A2, and A3 (Table 1). This aspect was the first subjective decision-making under the first reference point.

Table 1: Attribute values for three alternatives.

	C_1	C_2 (yuan)	C_3 (yuan)	C_4
$A1$	G	220,000	200,000–250,000	VG
$A2$	VG	250,000	240,000–300,000	C
$A3$	C	150,000	150,000–190,000	G

Step 4: We make use of the effect of unfavorable information on reference point adaptation to promote the manager's reference point adaptation. We informed the manager that the furniture market will go down in the next few years. The manager was asked again regarding his expectations toward the four factors. This aspect was set as the second reference point of the manager.

Step 5: We asked the manager to reorder the three alternatives. This aspect was the second subjective decision-making under the first reference point.

5.2. Experimental Analysis. Table 2 shows that in the subjective assignment of weights, geographical location was assigned the weight of 50%. The manager believed that geographical location is an important factor in opening furniture stores because a good geographical location can increase sales. The weights of the other three factors were 30%, 15%, and 5%. In the experiment, "the market of this industry will go down next year" is regarded as unfavorable information. Before the unfavorable information was provided, the manager's expectation for geographical location was very good. The expectation for annual rent was 240,000 yuan/year, that for decoration cost was between 250,000 and 280,000 yuan, and that for the transfer of the store was common. This aspect was set as the first reference point of the manager. After the unfavorable information was provided, the manager's expectation for geographical location was good. The expectation for annual rent was 200,000 yuan/year, that for decoration cost was between 220,000 and 260,000 yuan, and that for the transfer of the store was good. This aspect was set as the second reference point of the manager.

Under the first reference point, the manager chose the second alternative as the best one. After reference point adaptation, the manager's best choice was the first alternative. We then calculate the weight and reference point data in the DHMADM model and compare the results with the manager's subjective ranking of alternatives.

5.3. Data Analysis. $Q_j = \{q_j^1, q_j^2, \ldots, q_j^k\}$ is normalized into $Z_j^t = \{z_j^1, z_j^2, \ldots, z_j^k\}$. Decision matrix $X = [x_{ij}]_{m\times n}$ is normalized into $Y = [y_{ij}]_{m\times n}$. The normalized matrix with reference point 1 is Z^1 by using equations (2)–(13):

$$Z^1 = \{(0.75, 1.00, 1.00), 0.07, [0.13, 0.33], (0.25, 0.50, 0.75)\}. \tag{18}$$

Similarly, the normalized matrix of reference point 2 with three formats is Z^2. The purpose of doing so is to eliminate the influence of different dimensional units so as to facilitate the calculation and comparison of the comprehensive value of each alternative.

$$Z^2 = \{(0.50, 0.75, 1.00), 0.33, [0.27, 0.53], (0.50, 0.75, 1.00)\}. \tag{19}$$

The decision matrix is normalized by using equations (2)–(13):

$$Y = \left[y_{ij}\right]_{m\times n} = \begin{bmatrix} (0.50, 0.75, 1.00) & 0.20 & [0.33, 0.67] & (0.75, 1.00, 1.00) \\ (0.75, 1.00, 1.00) & 0.00 & [0.00, 0.40] & (0.25, 0.50, 0.75) \\ (0.25, 0.50, 0.75) & 0.67 & [0.73, 1.00] & (0.50, 0.75, 1.00) \end{bmatrix}. \tag{20}$$

The distance matrix for the first reference point is constructed by using equation (14):

$$D_1 = \begin{bmatrix} -0.20 & 0.13 & 0.27 & 0.43 \\ 0.00 & -0.07 & -0.11 & 0.00 \\ -0.43 & 0.60 & 0.63 & 0.25 \end{bmatrix}. \tag{21}$$

And similarly, the relative distance of z_j^2 and y_{ij} is D_2:

$$D_2 = \begin{bmatrix} 0.00 & -0.13 & 0.11 & 0.43 \\ 0.20 & -0.33 & -0.21 & -0.25 \\ -0.25 & 0.33 & 0.47 & 0.00 \end{bmatrix}. \tag{22}$$

The prospect values of each attribute relative to the first reference point can be computed by using equation (15). And the prospect decision matrix is as follows:

$$F_1 = \begin{bmatrix} -0.56 & 0.17 & 0.32 & 0.48 \\ 0.00 & -0.21 & -0.31 & 0.00 \\ -1.08 & 0.64 & 0.67 & 0.30 \end{bmatrix}. \tag{23}$$

Correspondingly, the value of the prospect value function relative to reference point 2 is F_2. And the prospect decision matrix is as follows:

$$F_2 = \begin{bmatrix} 0.00 & -0.38 & 0.13 & 0.48 \\ 0.25 & -0.86 & -0.57 & 0.48 \\ -0.66 & 0.38 & 0.57 & 0.00 \end{bmatrix}. \tag{24}$$

Comprehensive prospect value is the final value judgment combining the attribute of the alternative and the expectation of the DMs. The comprehensive prospect value of each alternative based on reference point adaptation can be calculated according to equations (16) and (17).

Table 2: Subjective weights, reference points, and alternative ranking of the manager.

Questions	Answers
(1) If you are ready to open a new furniture store, with a total of 10 points, how many points would you give to each of the following factors: geographical location C_1, annual rent C_2, decoration cost C_3, and transfer C_4?	C_1: 0.5 C_2: 0.3 C_3: 0.15 C_4: 0.05
(2) What are your expectations for the aforementioned factors?	C_1: VG C_2: 240,000 yuan/year C_3: 250,000–280,000 yuan C_4: C
(3) Please rank the following three alternatives.	$A_2 > A_1 > A_3$
(4) The information shows that the market of this industry will go down next year. When considering opening new stores, what are the expectations for the aforementioned four factors?	C_1: G C_2: 200,000 yuan/year C_3: 220,000–260,000 yuan C_4: G
(5) On the basis of learning this information, please reorder the three alternatives in the table according to your preference.	$A_1 > A_3 > A_2$

Reference point 1: $U(A_1) = -0.15$, $U(A_2) = -0.11$, and $U(A_3) = -0.23$

Reference point 2: $U(A_1) = -0.07$, $U(A_2) = -0.20$, and $U(A_3) = -0.14$

When the data of the first reference point are substituted into the model calculation, the results of the model calculation show that the manager's best choice is the second alternative. Moreover, when we substitute the data of the second reference point into the model for recalculation, the results show that the manager's best choice is the first alternative. This result is consistent with the manager's subjective decision-making. This means that under the influence of information, the reference point of DMs has changed, which affects the final decision-making of DMs. The DHMADM model just obtains the same conclusion, which reflects the final decision-making state of DMs.

5.4. Comparative Analysis. We compare the DHMADM model calculation results with the HMADM model calculation results. The HMADM model only considers a static reference point. In the DHMADM model, not only reference point 1 of the DMs is considered, but also reference point 2 of the DMs is affected by the unfavorable information.

As is shown in Table 3, the HMADM model calculation results show that if only the static reference points are considered, then the optimal choice of DMs is the second alternative, but in experiment result, DMs finally choose the first alternative as the best one. On the contrary, if the dynamic reference point is considered in the DHMADM model, the optimal choice of DMs calculated by the model is the first alternative. And this result is consistent with the real optimal decision of the DMs in the experiment.

Table 3: Comparison of HMADM and DHMADM model calculation results.

	HMADM model	DHMADM model
Model calculation results	$\mathbf{A}_2 > A_1 > A_3$	$\mathbf{A}_1 > A_2 > A_3$
Subjective ranking results	$A_2 > A_1 > A_3$	$\mathbf{A}_1 > A_3 > A_2$

The DMs' subjective attribute ranking and model calculation results show that under the influence of unfavorable information, decision-making changes when DMs' reference points adaptation. Meanwhile, subjective ranking results reflect decision-making results intuitively and truthfully. Comparing subjective ranking results with model calculation results is an important way to test the rationality of the model. Table 3 also shows that the subjective optimal alternative is consistent with the model calculation results in the DHMADM model. From the subjective judgment and calculation of the objective model, we can clearly observe the influence of changes in reference points on the decision-making results by establishing the DHMADM model with reference point adaptation as the core element.

If only reference point 1 is considered, the model in this paper is a HMADM model; if both reference point 1 and reference point 2 are considered, the model in this paper is a DHMADM model; by comparing the calculation results between those models, we found that the changes in reference points lead to changes in decision results. Furthermore, the practicality and effectiveness of the DHMADM model can be obtained by the consistency of the subjective judgment results and the objective calculation results of the model.

6. Conclusions

Making optimum decisions is important in a competitive environment. Prospect theory is a descriptive theory. Such theory is based on bounded rationality. In prospect theory, the reference point decides an individual's feeling of gain and loss [43]. Reference point adaptation causes changes in risk attitude and subsequent decision-making. This work establishes a DHMADM model on the basis of reference point adaptation. The attributes of the alternatives and reference points are described by real numbers, interval numbers, and linguistic variables. Under the effect of unfavorable information, the optimal choice of the DMs changes with the reference point adaptation. The model and method of calculation is also practical and effective.

Unfavorable information affects reference point adaptation and the subsequent decision-making. If only the static reference point is considered, then the optimal choice of DMs is the second alternative in the model calculation, but the DMs finally choose the first alternative as the best one in experiment result. This means that only considering the static reference point cannot accurately reflect the actual decision-making situation of the DM. On the contrary, if the dynamic reference point is considered in the DHMADM model, the optimal choice of DMs calculated by the model is

the first alternative. The results of the DHMADM model are consistent with the subjective representation of DM. Prior to receiving unfavorable information, DMs would choose a very good geographical store location. However, after determining that the industry outlook for the next year is unfavorable, the manager chooses to find a good geographical store location with cheaper rent. The change of decision result accompanied by this psychological change of DM is appropriately expressed through the HDMADM model.

The choice of DMs' subjective optimal alternative is consistent with the model calculation result before and after reference point adaptation. The subjective optimal alternative of DMs before reference point adaptation is the second one. Under the influence of the unfavorable information, the reference point and optimal alternative of DMs change. In the model calculation, before receiving the unfavorable information, the DMs' optimal choice is the second alternative. After receiving the unfavorable information, the DMs' optimal choice is the first alternative. Therefore, the accuracy of the DHMADM model is obtained by comparing the experimental and model data results.

The complexity of the socio-economic environment can be effectively reflected by constructing a DHMADM model on the basis of reference point adaptation. This study has certain limitations. The main limitation of this research is the lack of a reference point adaptation model because the dynamic reference point model varies under different environments. The other limitation is that the reference point is a subjective factor, so the data of the reference point can only be obtained through the subjective expression of DMs. Then, it is hard to compare this model with other models except the HMADM model in this paper. While the consistency of the subjective judgment results and the objective calculation results also can illustrate the practicality of the DHMADM model. The future DHMADM model can involve deviation attributes, such as fuzzy and soft sets.

Data Availability

No data were used to support this study.

Conflicts of Interest

The authors declare that they have no conflicts of interest.

References

[1] C. Wang, Z. Ji, and Y. Wang, "Many-objective flexible job shop scheduling using NSGA-III combined with multi-attribute decision making," *Modern Physics Letters B*, vol. 32, no. 34–36, 2018.

[2] A. Baykasoğlu and İ. Gölcük, "Development of an interval type-2 fuzzy sets based hierarchical MADM model by combining DEMATEL and TOPSIS," *Expert Systems with Applications*, vol. 70, pp. 37–51, 2017.

[3] Z. K. Azadeh and K. Adem, "Multi-attribute decision-making based on soft set theory: a systematic review," *Soft Computing*, vol. 23, no. 16, pp. 6899–6920, 2019.

[4] Z. Yue, "A method for group decision-making based on determining weights of decision makers using TOPSIS," *Applied Mathematical Modelling*, vol. 35, no. 4, pp. 1926–1936, 2011.

[5] K.-Y. Shen, S.-K. Hu, and G.-H. Tzeng, "Financial modeling and improvement planning for the life insurance industry by using a rough knowledge based hybrid MCDM model," *Information Sciences*, vol. 375, pp. 296–313, 2017.

[6] L. Zhong and L. Yao, "An ELECTRE I-based multi-criteria group decision making method with interval type-2 fuzzy numbers and its application to supplier selection," *Applied Soft Computing*, vol. 57, pp. 556–576, 2017.

[7] J. Qin, X. Liu, and W. Pedrycz, "An extended TODIM multi-criteria group decision making method for green supplier selection in interval type-2 fuzzy environment," *European Journal of Operational Research*, vol. 258, no. 2, pp. 626–638, 2017.

[8] Z. L. Yue, "An avoiding information loss approach to group decision making," *Applied Mathematical Modelling*, vol. 37, no. 1-2, pp. 112–126, 2013.

[9] G. Wei, "Grey relational analysis model for dynamic hybrid multiple attribute decision making," *Knowledge-Based Systems*, vol. 24, no. 5, pp. 672–679, 2011.

[10] J. Ye, "Correlation coefficient between dynamic single valued neutrosophic multisets and its multiple attribute decision-making method," *Information*, vol. 8, no. 2, p. 41, 2017.

[11] T. Yang, M.-C. Chen, and C.-C. Hung, "Multiple attribute decision-making methods for the dynamic operator allocation problem," *Mathematics and Computers in Simulation*, vol. 73, no. 5, pp. 285–299, 2007.

[12] J. H. Park, H. J. Cho, and Y. C. Kwun, "Extension of the VIKOR method to dynamic intuitionistic fuzzy multiple attribute decision making," *Computers & Mathematics with Applications*, vol. 65, no. 4, pp. 731–744, 2013.

[13] Z. Xu, "On multi-period multi-attribute decision making," *Knowledge-Based Systems*, vol. 21, no. 2, pp. 164–171, 2008.

[14] L. He and H. Teng, "GRA model for dynamic hybrid multiple attribute decision making," *Journal of Intelligent & Fuzzy Systems*, vol. 27, no. 2, pp. 1067–1075, 2014.

[15] J.-M. Shen, Y.-G. Dang, W.-J. Zhou, and X.-M. Li, "Evaluation for core competence of private enterprises in Xuchang city based on an improved dynamic multiple-attribute decision-making model," *Mathematical Problems in Engineering*, vol. 2015, Article ID 493240, 10 pages, 2015.

[16] F. Y. Ai and J. Y. Yang, "Approaches to dynamic multiple attribute decision making with 2-tuple linguistic information," *Journal of Intelligent & Fuzzy Systems*, vol. 27, no. 6, pp. 2715–2723, 2014.

[17] Y. Liu, "A method for 2-tuple linguistic dynamic multiple attribute decision making with entropy weight," *Journal of Intelligent & Fuzzy Systems*, vol. 27, no. 4, pp. 1803–1810, 2014.

[18] Z.-X. Su, M.-Y. Chen, G.-P. Xia, and L. Wang, "An interactive method for dynamic intuitionistic fuzzy multi-attribute group decision making," *Expert Systems with Applications*, vol. 38, no. 12, pp. 15286–15295, 2011.

[19] L. Xiao, D. Xu, C. Xie, N. B. Mandayam, and H. V. Poor, "Cloud storage defense against advanced persistent threats: a prospect theoretic study," *IEEE Journal on Selected Areas in Communications*, vol. 35, no. 3, pp. 534–544, 2017.

[20] L. Wang, Z.-X. Zhang, and Y.-M. Wang, "A prospect theory-based interval dynamic reference point method for emergency decision making," *Expert Systems with Applications*, vol. 42, no. 23, pp. 9379–9388, 2015.

[21] L. Xiao, N. B. Mandayam, and H. Vincent Poor, "Prospect theoretic analysis of energy exchange among microgrids," *IEEE Transactions on Smart Grid*, vol. 6, no. 1, pp. 63–72, 2015.

[22] Z.-P. Fan, X. Zhang, F.-D. Chen, and Y. Liu, "Multiple attribute decision making considering aspiration-levels: a method based on prospect theory," *Computers & Industrial Engineering*, vol. 65, no. 2, pp. 341–350, 2013.

[23] L. Y. Peng, P. D. Liu, and Z. M. Liu, "Research on the random multi-attribute decision-making methods with trapezoidal fuzzy probability based on prospect theory," *Journal of Intelligent & Fuzzy Systems*, vol. 26, no. 5, pp. 2131–2141, 2014.

[24] X. Li and X. Chen, "Extension of the TOPSIS method based on prospect theory and trapezoidal intuitionistic fuzzy numbers for group decision making," *Journal of Systems Science and Systems Engineering*, vol. 23, no. 2, pp. 231–247, 2014.

[25] S. Liu and X. Liu, "A sample survey based linguistic MADM method with prospect theory for online shopping problems," *Group Decision and Negotiation*, vol. 25, no. 4, pp. 749–774, 2016.

[26] Y. Li and D. Zhang, "Dynamic multi-attribute decision-making method with three-parameter interval grey number based on the prospect theory," *Grey Systems: Theory and Application*, vol. 8, no. 4, pp. 424–435, 2018.

[27] J. Zhu, Z. Ma, H. Wang, and Y. Chen, "Risk decision-making method using interval numbers and its application based on the prospect value with multiple reference points," *Information Sciences*, vol. 385-386, pp. 415–437, 2017.

[28] W. F. Dai, Q. Y. Zhong, and C. Z. Qi, "Multi-stage multi-attribute decision-making method based on the prospect theory and triangular fuzzy MULTIMOORA," *Soft Computing*, no. 2, , 2018.

[29] P. Liu, F. Jin, X. Zhang, Y. Su, and M. Wang, "Research on the multi-attribute decision-making under risk with interval probability based on prospect theory and the uncertain linguistic variables," *Knowledge-Based Systems*, vol. 24, no. 4, pp. 554–561, 2011.

[30] H. Chen and A. R. Rao, "Close encounters of two kinds: false alarms and dashed hopes," *Marketing Science*, vol. 21, no. 2, pp. 178–196, 2002.

[31] H. R. Arkes, D. Hirshleifer, and S. Lim, "Reference point adaptation: tests in the domain of security trading," *Organizational Behavior and Human Decision Processes*, vol. 105, no. 1, pp. 67–81, 2008.

[32] H. R. Arkes, D. Hirshleifer, D. Jiang, and S. S. Lim, "A cross-cultural study of reference point adaptation: evidence from China, Korea, and the US," *Organizational Behavior and Human Decision Processes*, vol. 112, no. 2, pp. 99–111, 2010.

[33] M. Baucells, M. Weber, and F. Welfens, "Reference-point formation and updating," *Management Science*, vol. 57, no. 3, pp. 506–519, 2011.

[34] Y. Shi, X. Cui, J. Yao, and D. Li, "Dynamic trading with reference point adaptation and loss aversion," *Operations Research*, vol. 63, no. 4, pp. 789–806, 2015.

[35] D. Kahneman, "Maps of bounded rationality: psychology for behavioral economics," *American Economic Review*, vol. 93, no. 5, pp. 1449–1475, 2003.

[36] K. A. Tversky, "Prospect theory: an analysis of decision under risk," *Econometrica*, vol. 47, no. 2, pp. 263–292, 1979.

[37] B. Bartling, L. Brandes, and D. Schunk, "Expectations as reference points: field evidence from professional soccer," *Management Science*, vol. 61, no. 11, pp. 2646–2661, 2015.

[38] W. M. Ma, H. Zhang, and N. L. Wang, "Improving outpatient satisfaction by extending expected waiting time," *BMC Health Services Research*, vol. 19, no. 1, 2019.

[39] A. Peysakhovich and U. R. Karmarkar, "Asymmetric effects of favorable and unfavorable information on decision making under ambiguity," *Management Science*, vol. 62, no. 8, pp. 2163–2178, 2016.

[40] Z. P. Fan, F. D. Chen, and X. Zhang, "Method for hybrid multiple attribute decision making method based on cumulative prospect theory," *Journal of Systems Engineering*, vol. 27, no. 3, pp. 295–301, 2012.

[41] C.-S. Ying, Y.-L. Li, K.-S. Chin, H.-T. Yang, and J. Xu, "A new product development concept selection approach based on cumulative prospect theory and hybrid-information MADM," *Computers & Industrial Engineering*, vol. 122, pp. 251–261, 2018.

[42] Z. Yue and Y. Jia, "A group decision making model with hybrid intuitionistic fuzzy information," *Computers & Industrial Engineering*, vol. 87, pp. 202–212, 2015.

[43] K. A. Sullivan, E. Uchida, T. W. Sproul, and J. Xu, "Prospect theory and tenure reform: impacts on forest management," *Land Economics*, vol. 94, no. 3, pp. 405–424, 2018.

Hindawi
Mathematical Problems in Engineering
Volume 2019, Article ID 9619282, 11 pages
https://doi.org/10.1155/2019/9619282

Research Article

Airflow Patterns around Obstacles with Large-Span Shallow Shell Roof: Wind Tunnel Measurements and Direct Simulation

Hongying Jia, Huixue Dang, Qianying Ma, and Jun-Hai Zhao

School of Civil Engineering, Chang'an University, Xi'an 710061, China

Correspondence should be addressed to Huixue Dang; dhxlxz@126.com

Received 8 June 2019; Revised 7 October 2019; Accepted 18 October 2019; Published 15 November 2019

Guest Editor: Miguel G. Torres

Wind tunnel tests on the rigid model of large-span shallow spherical shell roof structure were carried out. The variation rule and the calculation method for the average shape coefficient of the fluctuating wind pressure under six different typical wind directions were obtained. The wind pressure distribution of the node deflection and cross section stress was numerically investigated and analyzed. Meanwhile, the effect of mechanics-flow form of the typical spherical shell structure on the wind pressure distribution was analyzed quantitatively. In this study, it is found that the results of numerical simulation agree well with the wind tunnel test data. The study on the mechanical characteristics, as well as the wind vibration research, of the spherical shell structure in different working conditions provides a reliable theoretical basis for the mechanical index of the wind vibration.

1. Introduction

Large-span roof structure has been widely used for various large public buildings such as hangars, gymnasiums, and exhibition pavilions in recent decades. The thin shell structure is considered as a great technological progress compared with the large-span roof structure because they can cover a large free area with a roof having a thickness of only a few centimeters [1]. A thin shell is defined as a three-dimensional spatial curved structural surface that is composed of one or more folded plates and curved slabs. Thin shell is recognized as the form-resistant structure that mainly produces bending moment and in-plane stress when subjected to external loads [2, 3]. Due to the aesthetically pleasing surface and reasonable structural form, the shell structure has been widely employed since 1960s. Because of the high strength-to-weight and stiffness-to-weight ratios of these structures and considering the complexity of structural dynamic characteristics, the research on the susceptibility of shell roof subjected to wind loads is of great importance.

Some investigations on the wind-induced dynamic response and stress distribution of large-span roof structures have been performed. Full-scale wind pressure measurement on single-span buildings was conducted by Hoxey and Robertson [4], which indicated that the geometric shape of structure had obvious influences on the wind-induced response of structure. Uematsu et al. [5] studied the wind load characteristics and the mean and fluctuating wind pressures of latticed dome. Fu et al. [6] investigated the effect of wind speed, wind direction, and acceleration responses on the structural performance of roof structures.

Compared with high-rise vertical buildings, the large-span roof structure is featured with its complicated structural frequencies and dynamic resonant responses [7, 8]. Moreover, it is rather complicate to grasp vibration modes of large-span roof structures. Therefore, the extremum of wind-induced responses of large-span shell roof structures cannot be produced only by numerical methodologies. In fact, every single structure has its own special characteristics, and wind tunnel tests of a scaled model are considered essential in order to accurately assess the effect of wind pressure on the large-span structure [9]. Typically, wind tunnel tests are employed to obtain information considering the vibration response or the wind pressure distribution of structures due to the applied wind. Marukawa et al. [10] conducted a series of wind tunnel tests regarding the issue of

fluctuating wind pressures. They discussed the gust loading factor of the large-span roof structures. Hongo [11] investigated the effect of spherical roof's geometry on the characteristics of the wind pressure field in a wind tunnel, and then an empirical formula for assessing the design wind loads was developed. Zhou et al. [12] obtained the experimental tests upon means and fluctuating wind pressures acting on a large roof structure through wind tunnel experiments.

In this study, to determine the mean and fluctuating wind load characteristics, a shallow spherical shell roof structure (with rise-to-span ratio less than 1/5) was investigated by a wind tunnel test on a scaled model. In addition, the wind pressure coefficient and fluctuating wind pressure under different typical wind directions were obtained. Moreover, ANSYS software and midas gen software were used to simulate the wind pressure filed of this shallow spherical shell roof structure under different wind directions. The wind-induced responses of this thin spherical shell roof structure provided detailed understanding and enriched corresponding database of large-span spatial roof structure.

2. Wind Tunnel Experiments

2.1. Test Setup. The experiments were conducted in a closed-type wind tunnel at Northwest University of Technology, China, which consists of three alterable sections with a total length of 80 m. Dimensions of the testing section employed are $12 \times 2.5 \times 3.5$ m (length × height × width, $L \times H \times W$). The wind-induced vibrations of spherical shell roof structure were predicted based on the wind tunnel experiment data, and the maximum permissible wind velocity was 90 m/s, and the minimum stable wind velocity was 10 m/s. The wind pressure was measured by the PSI9816 device and the network intelligent pressure data acquisition system based on TCP/TP. The outline of the wind tunnel is shown in Figure 1.

2.2. Experimental Model. The tested model was constructed at 1 : 100 scale by using glass materials with a thickness of 3 mm. The spherical shell roof in the experiment had a length of 0.083 m along the arrow height and 1 m in span, which means the rise-to-span is 1 : 12. The model was deployed on a wood plate with a diameter of 1.9 m, while smooth chamfers were designed around the wood plate. A total of 352 wind pressure measurement points were arranged on the half side of model considering the symmetric characteristic. The sampling frequency was 100 Hz. The air tightness of each pressure line was checked before the installation of the model. The distribution of pressure measurement points is shown in Figure 2.

The directions of wind were selected as 0°, ±45°, ±90°, and 180° (defined by the longitudinal axis of wind tunnel), while the geomorphology and wind profile were neglected in the test. The wind speed was 26.8 m/s.

The average wind pressure coefficient $C_{p,i}$ of each pressure tap under different wind directions was derived by

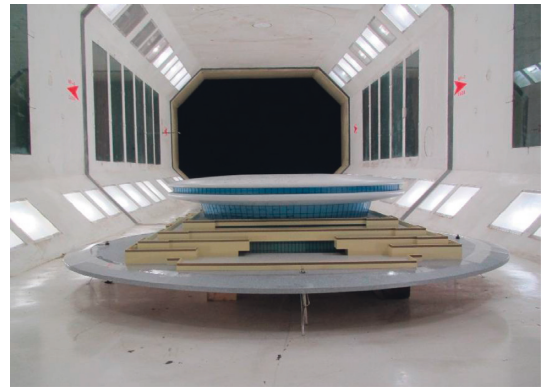

Figure 1: The wind pressure model in wind tunnel.

$$C_{p,i} = \frac{p_i - p_\infty}{(1/2)\rho v^2}, \tag{1}$$

where p_i = pressure at ith point, p_∞ = static pressure of the reference point, and $(1/2)\rho v^2$ = dynamic pressure of the reference point.

The local shape coefficient of model μ_z can be obtained by using wind load ω_k [13], basic wind pressure ω_0, vibration factor β_z, and height variation factor of wind pressure at height z μ_z.

$$\mu_s = \frac{\omega_k}{\omega_0 \cdot \beta_z \cdot \mu_z}, \tag{2}$$

where μ_z can be calculated as

$$\mu_z = 0.478 Z^{0.32}. \tag{3}$$

3. Experimental Results and Discussion

The wind pressure coefficients of six different wind directions are displayed in Figure 3, where m represents the number of pressure measurement points. It can be seen that the pressure of each pressure tap was varied with the change of wind direction, and it is obvious that in some specific areas of the model, the pressure coefficient reached a peak value of −2.5 while the coefficient of other area closed to zero. It is known that the non-full-span distribution of wind pressure possibly leads to more disadvantages on the mechanical performance of structures compared with the case of full-span distribution. Therefore, it is necessary to obtain the actual distribution of wind pressure on the complex structures. Seven replication experiments were conducted to achieve the coefficient of wind pressure under the wind direction of 0°, and the test results are shown in Table 1. It was obtained that the results of different experiments in the present study showed a relatively higher level of repeatability, which indicates that the results of present experimental investigation assumed typical response of thin spherical shell roof structures.

Figure 4 shows the local shape coefficients of the model under wind directions employed in this study according to equations (2) and (3). It is considered that the wind

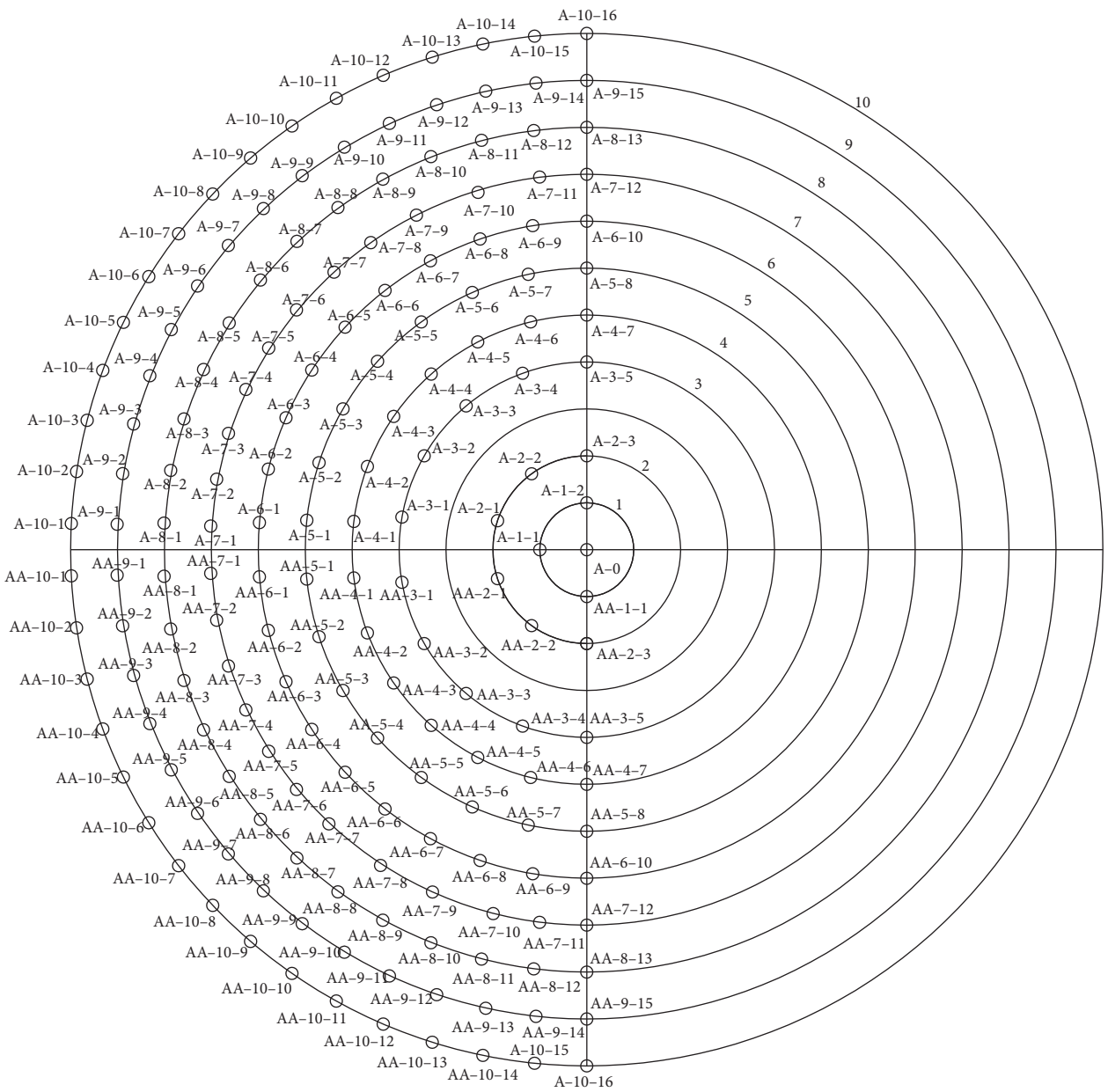

Figure 2: Pressure measurement points on the model.

pressure of the model appeared as suction forces upward owing to the negative value of wind pressure with the wind directions between 0 and 90 degrees, and the shape coefficients of the forward area of the model possessed a declination attributed to the separation zone in front of the roof. Simultaneously, the variation in shape coefficients of the backward of the model showed a smoothly increasing alteration as a result of the existence of reattachment zone at this area.

Figure 5 presents the pressure nephogram and isobaric line of the shallow shell spherical roof with different wind directions in the wind tunnel test. It was observed that the maximum suction forces of wind on the surface of roof occurred at the lateral side of edge on the upwind side, and it was worth noting that the distribution of wind pressure on the thin spherical shell roof differs from that of spherical shell roof; the separation of wind pressure was moderate owing to the relatively small suction force caused by wind.

Furthermore, wind pressures on the surface of shallow spherical shell roof were of negative values, and the wind load on the roof was dominated by suction forces, while the maximum suction force was observed at the top of the roof surface, which was induced by the flow acceleration along the curved surface at this area. In conclusion, the wind tunnel test suggests that the aerodynamic shape of shallow spherical shell roof can be improved to reduce the influence of wind load.

4. Finite Element (FE) Analysis

To compare the results from tests and the performance of unscaled structure, the finite element model of original

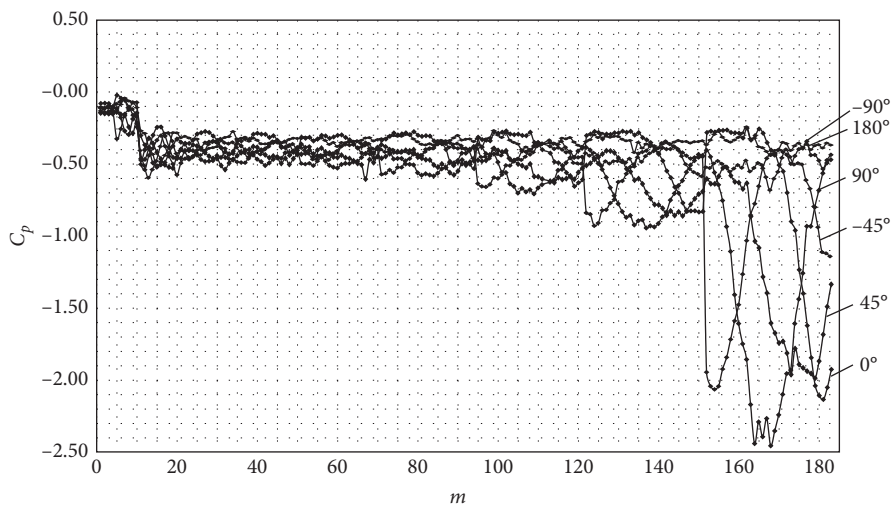

Figure 3: The wind pressure coefficient under six different wind directions.

Table 1: Seven repetitive test results under the wind direction of 0°.

Pressure taps	1	2	3	4	5	6	7
A-0	−0.079	−0.079	−0.078	−0.078	−0.080	−0.078	−0.079
A-9-15	−0.830	−0.831	−0.831	−0.830	−0.833	−0.830	−0.830
B-1-1	0.384	0.379	0.375	0.379	0.379	0.382	0.379
B-1-15	−0.564	−0.564	−0.564	−0.566	−0.566	−0.563	−0.563
C-1-12	0.833	0.832	0.833	0.833	0.832	0.827	0.832
C-3-9	−0.020	−0.023	−0.025	−0.025	−0.025	−0.023	−0.021
D-1-11	−0.581	−0.581	−0.583	−0.588	−0.581	−0.587	−0.583
D-2-12	−0.605	−0.609	−0.613	−0.616	−0.608	−0.612	−0.608

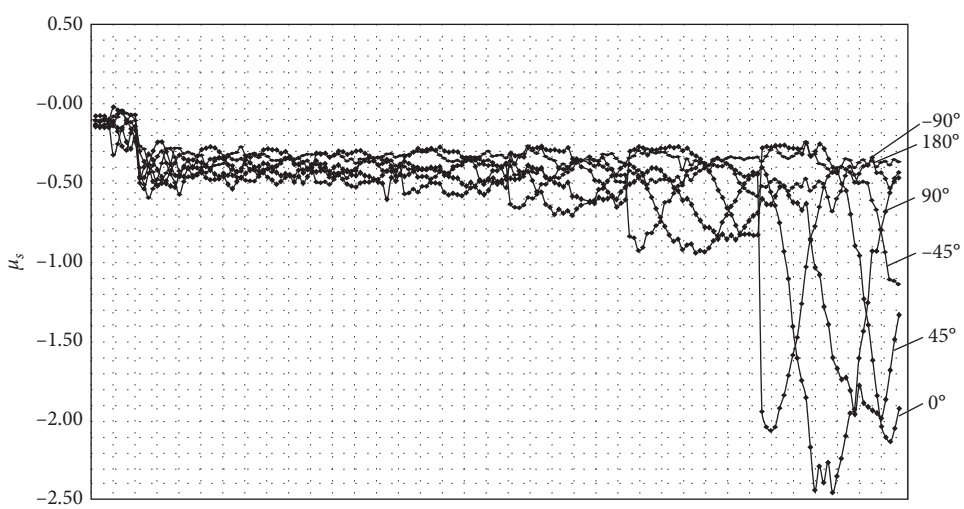

Figure 4: Local shape coefficients of the model. Wind direction of (a) 0°, (b) 45°, (c) 90°, (d) 180°, (e) −90°, and (f) −45°.

structure was developed by using the ANSYS software to obtain specific responses, as shown in Figure 6. The wind load was applied to the model according to the test.

Under Cartesian coordinates, the three-dimensional compressible unsteady Navier–Stokes equations in integral form can be written as

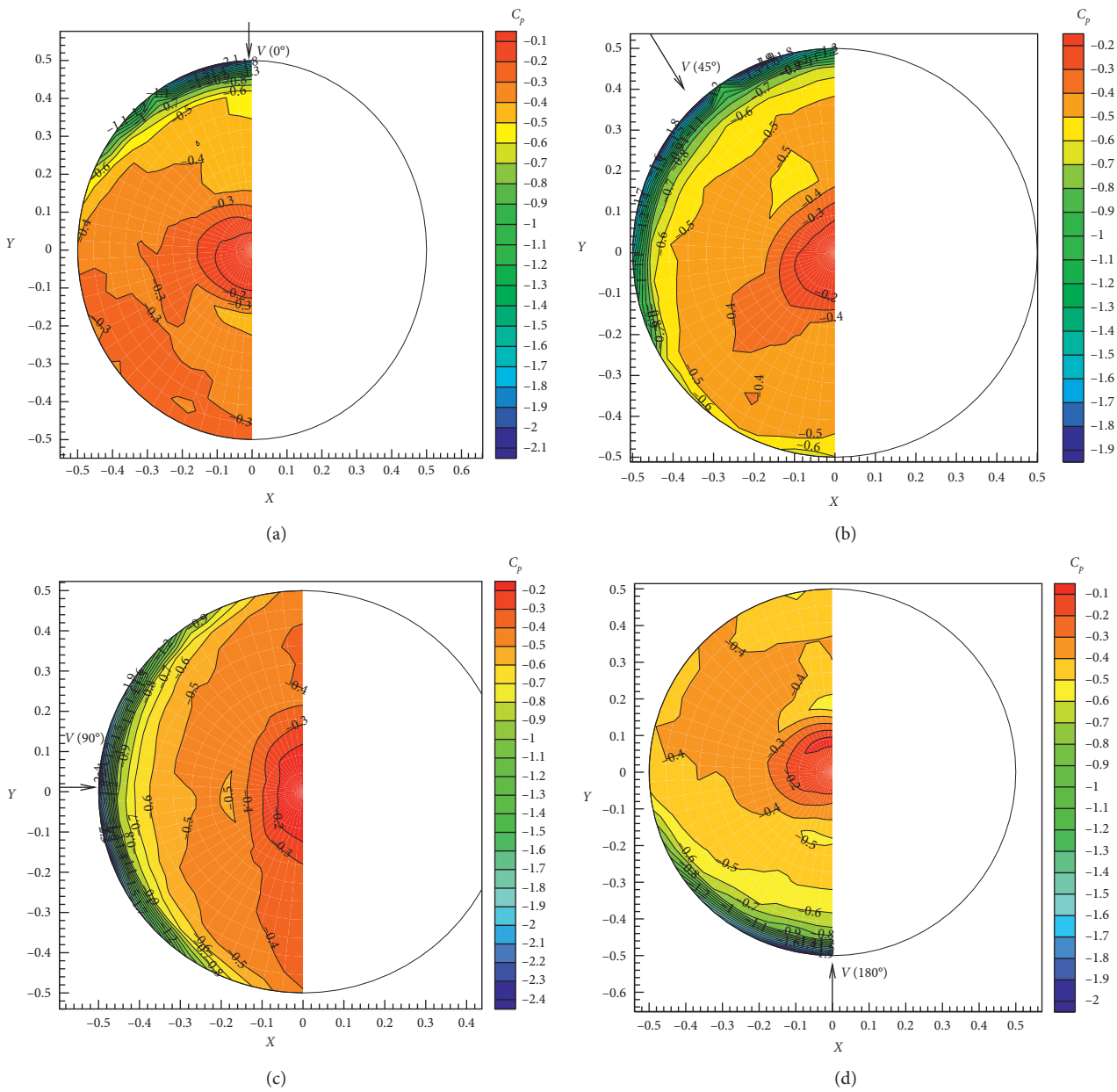

Figure 5: Continued.

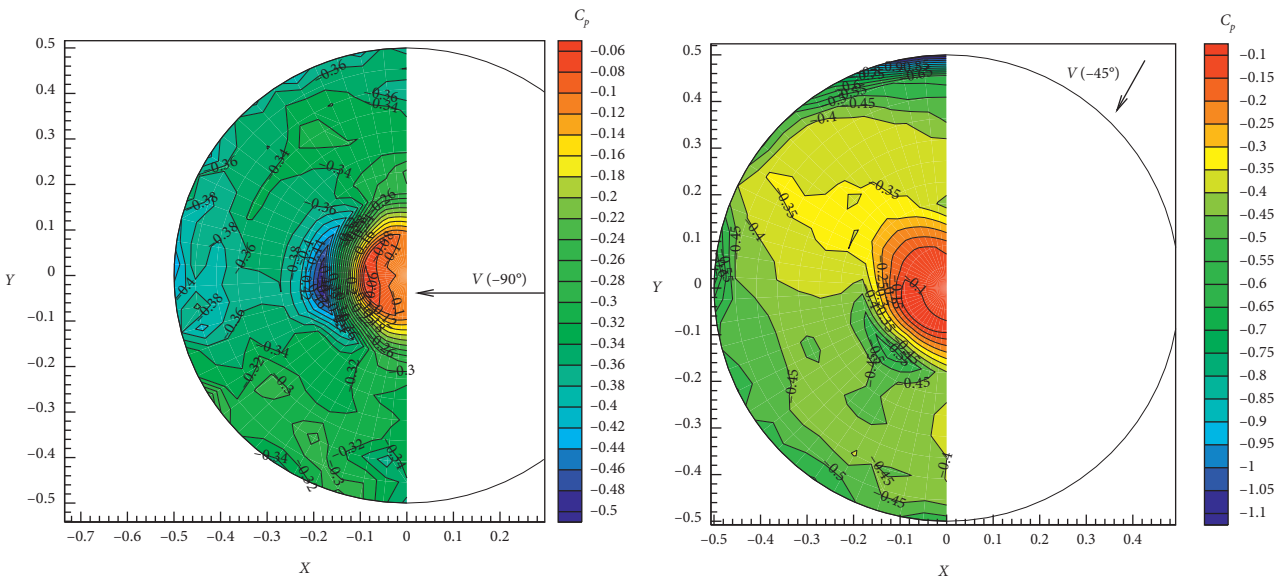

(e) (f)

Figure 5: The pressure nephogram and isobaric line of shallow shell spherical roof.

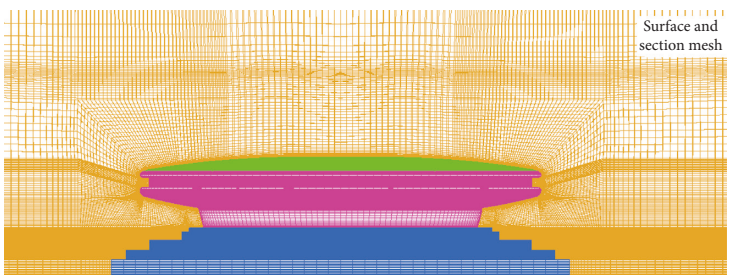

Figure 6: Finite element modelling of structure.

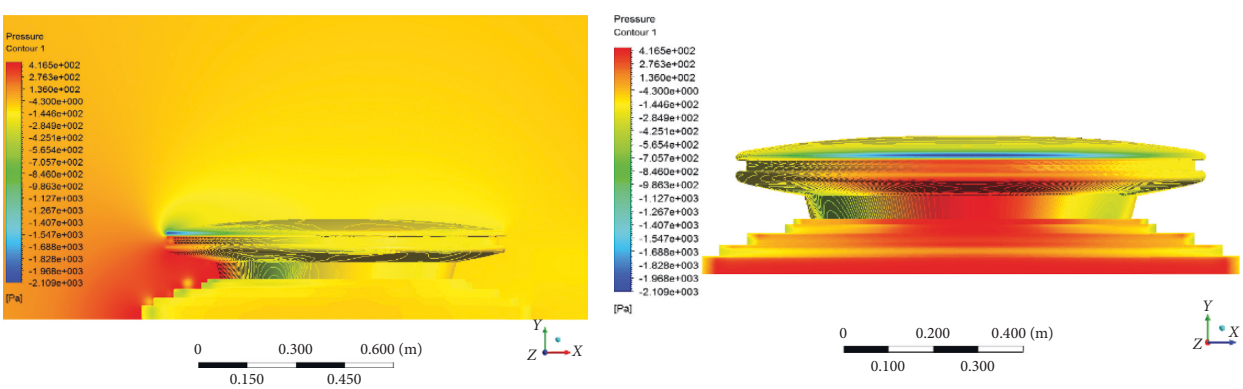

(a) (b)

Figure 7: Continued.

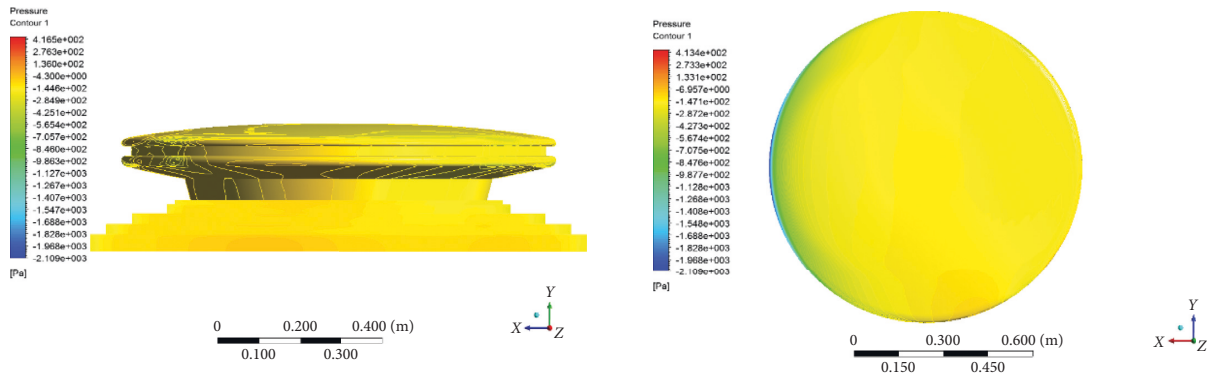

(c) (d)

Figure 7: Results of FE analysis. (a) Lateral side of the model. (b) Windward side. (c) Leeside of the model. (d) Shell roof.

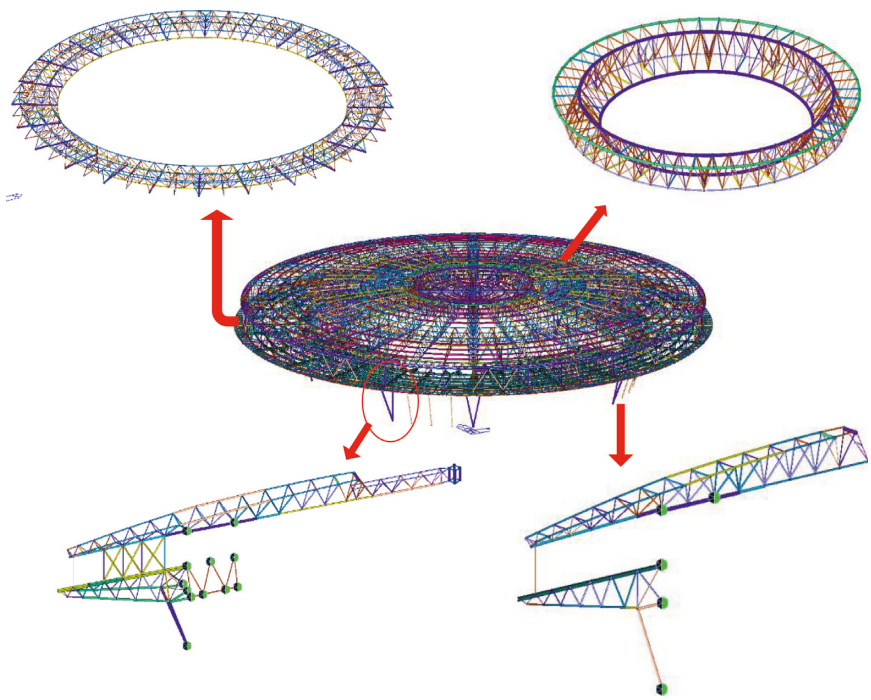

Figure 8: Finite element modelling of structure.

Table 2: Basic load conditions applied to the model.

Conditions	Type of load	Wind load (kN/m^2)
1	Dead load	1.13/1.83
2	Live load	0.5
3	Live load	4.5

Table 3: Results of modal analysis.

Modals	Frequency		Period (s)
	rad/s	Cycle/s	
1	6.9679	1.109	0.9017
2	7.8129	1.2435	0.8042
3	9.566	1.5225	0.6568
4	10.565	1.6815	0.5947
5	14.4582	2.3011	0.4346

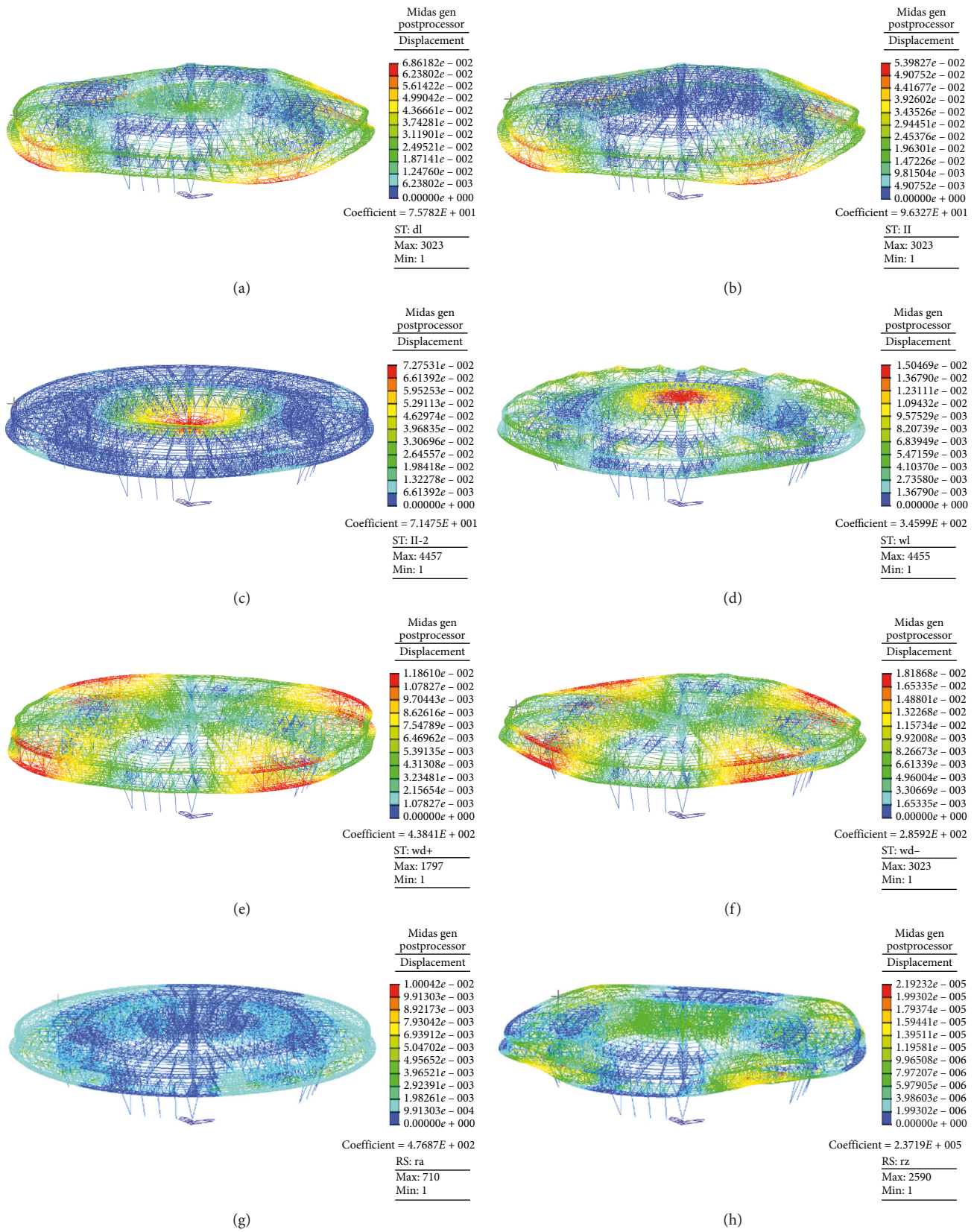

Figure 9: Displacements of nodes in the FE model under different load conditions. (a) Condition 1. (b) Condition 2. (c) Condition 3. (d) Condition of wind load. (e) Condition of increasing temperature. (f) Condition of decreasing temperature. (g) Condition of horizontal seismic. (h) Condition of horizontal seismic.

Table 4: Envelope values of stress in FE model under different load conditions.

Elements	σ_{max} (kN·m^{-2})	σ_{min} (kN·m^{-2})	Elements	σ_{max} (kN·m^{-2})	σ_{min} (kN·m^{-2})	Elements	σ_{max} (kN·m^{-2})	σ_{min} (kN·m^{-2})
90835	59.2	−63.5	91411	56.4	−65.8	91699	−42.0	−57.3
90837	26.0	−56.9	91413	25.2	−59.7	91700	−44.3	−68.3
90839	61.8	−33.4	91415	61.0	−39.0	91701	−25.5	−47.2
90841	81.7	15.1	91417	80.4	−12.0	91702	18.3	−30.7
90843	144.0	51.3	91419	143.0	42.8	91703	54.0	9.2
90845	205.0	24.6	91421	205.0	17.0	91704	103.0	−19.9
90846	146.0	−67.1	91422	146.0	−73.7	92250	−41.7	−80.4
90849	122.0	−91.4	91425	122.0	−96.5	92257	−49.1	−63.2
90852	79.8	−34.0	91428	78.8	−39.3	92258	−41.5	−55.4
90855	70.0	53.1	91431	69.0	47.6	92259	−22.6	−49.5
90858	61.4	59.3	91434	59.4	55.7	92260	21.5	−33.1
90861	61.3	30.3	91437	60.4	26.6	92261	58.5	7.9
90864	21.7	−30.3	91440	20.9	−32.8	92262	107.0	−17.7
90865	−19.1	−67.6	91441	−19.6	−69.4			

Table 5: Envelope values of displacements of nodes in the FE model under different load conditions.

Nodes	δ_x (mm)	δ_y (mm)	δ_z (mm)	Nodes	δ_x (mm)	δ_y (mm)	δ_z (mm)
5403	−0.56	0.20	−11.64	7062	0.26	0.27	−6.32
5406	−0.70	0.22	−10.38	7063	0.43	0.27	−5.03
5409	−0.81	0.23	−9.16	7064	0.65	0.26	−3.98
5412	−0.95	0.21	−7.41	7213	0.32	0.22	−14.4
5413	−0.82	0.23	−5.15	7215	0.49	0.22	−13.4
5415	−1.04	0.09	−5.48	7231	1.10	0.12	−4.34
5474	0.18	0.27	−7.97	7233	0.93	0.16	−3.59
5475	−0.09	0.26	−6.48	7247	−0.09	0.28	−9.06
5476	−0.26	0.26	−5.12	7268	−0.18	0.28	−10.2
5477	−0.49	0.24	−4.00	9525	0.61	1.27	−3.23
5597	−0.21	0.18	−14.08	9546	0.07	0.32	−10.8
5598	−0.37	0.18	−13.05	9572	0.05	0.29	−14.0
5711	0.26	0.27	−9.33	9573	0.03	0.30	−13.5
5712	0.36	0.25	−10.50	9589	0.11	0.28	−14.1
5714	−0.77	0.13	−3.55	9593	0.14	0.28	−13.7
6997	0.69	0.24	−11.94	9636	0.03	0.30	−12.5
6999	0.83	0.26	−10.65	9638	0.06	0.31	−11.5
7003	0.95	0.27	−9.39	9684	0.15	0.28	−12.8
7005	1.09	0.25	−7.59	9685	0.12	0.30	−11.8
7009	1.19	0.13	−5.62	9772	0.07	0.30	−14.1
7061	0.12	0.28	−7.75	9776	0.09	0.28	−14.1

$$\frac{\partial}{\partial t}\iiint_{\Omega}\mathbf{Q}\,\mathrm{d}V + \oiint_{\partial\Omega}\mathbf{F}\cdot\vec{\mathbf{n}}\,\mathrm{d}S = 0, \tag{4}$$

where $\mathbf{Q} = (\rho, \rho u, \rho v, \rho w, \rho e)^T$ denotes the solution vector, $\partial\Omega$ denotes the boundary of integral domain, $\vec{\mathbf{n}}$ denotes the normal vector directing outward of integral domain, and t is time.

To well capture the unsteady boundary layer separation induced by shockwave in transonic flow, the shear stress transport (SST) k-ω turbulence model is chosen to enclose Navier–Stokes equations for steady state simulations. The transport equations for turbulence energy k and dissipation rate ω can be written as follows:

$$\begin{aligned}\frac{\partial(\boldsymbol{\rho}\mathbf{k})}{\partial\mathbf{t}} + \frac{\partial(\boldsymbol{\rho}\mathbf{k}\mathbf{u}_\mathbf{i})}{\partial\mathbf{x}_\mathbf{i}} &= \frac{\partial}{\partial\mathbf{x}_\mathbf{j}}\left(\Gamma_\mathbf{k}\frac{\partial\mathbf{k}}{\partial\mathbf{x}_\mathbf{j}}\right) + \widetilde{\mathbf{G}}_\mathbf{k} - \mathbf{Y}_\mathbf{k},\\ \frac{\partial(\boldsymbol{\rho}\boldsymbol{\omega})}{\partial\mathbf{t}} + \frac{\partial(\boldsymbol{\rho}\boldsymbol{\omega}\mathbf{u}_\mathbf{i})}{\partial\mathbf{x}_\mathbf{i}} &= \frac{\partial}{\partial\mathbf{x}_\mathbf{j}}\left(\Gamma_\boldsymbol{\omega}\frac{\partial\boldsymbol{\omega}}{\partial\mathbf{x}_\mathbf{j}}\right) + \mathbf{G}_\boldsymbol{\omega} - \mathbf{Y}_\boldsymbol{\omega} + \mathbf{D}_\boldsymbol{\omega}.\end{aligned} \tag{5}$$

For both inviscid and viscous terms in Navier–Stokes equations, the second-order upwind scheme proposed by Barth and Jesperson is employed.

Figure 7 presents the results of FE analysis. The wind pressure yields greater values between the shell roof and the ground, while the wind appeared to separate at the steps, leading to the vortex in the form of low pressure. Due to blunt body of the model, the pressure in the middle position is the highest, with the flow of air from the middle to both sides and above; the pressure gradually decreases, and the change of pressure is directly related to the local windward area, and under the condition of flow separation, the pressure recovery on the leeward side is low, and the total pressure on the leeward side is lower than that on the upwind side. On the windward side of the top cover, the effect of flow around is more obvious; while moving from the symmetrical position to both sides, the effect of flow acceleration gradually weakens. By making comparisons between Figures 7 and 5, it can be concluded that distributions

of wind pressure obtained by FE method and tests are similar, which somewhat confirms the validity of FE analysis.

The midas gen software was used to simulate the response of unscaled structure. The truss element was employed to establish the finite element model, as shown in Figure 8. The dead loads and live loads are selected according to the practical engineering, yet the deadweight of structure was not included.

The wind load ω_k was calculated by equation (2), where μ_z was taken as 1.7 in accordance with the test results, and μ_s, μ_z, and ω_0 were determined according to GB 50009-2012 [13].

Three load conditions, including dead loads, live loads, seismic loads, and wind loads, were applied to the model to conduct the finite element analysis. The specific information of basic load conditions is listed in Table 2. Specially, for the purpose of considering the seismic action, the modal analysis was carried out in order to transfer seismic loads into static forces, and the results are organized in Table 3. Moreover, the influence of temperature change on the structure was taken into consideration, and ranges of 15–30 and 8–15 degrees were selected as cases for temperature change.

The node displacements of finite element (FE) model under three load conditions, seismic loads, and temperature loads are shown in Figure 9. It was concluded that the performance of structure under each single load condition is favorable on the basis of the limited displacement of nodes in the FE model. So, combinations of these load conditions were made to investigate the performance of the structure under various load conditions. The combinations of loads are referred to the form as

$$\lambda_t = \eta_1\lambda_1 + \eta_2\lambda_2 + \eta_3\lambda_3 + \eta_4\lambda_4 + \eta_5\lambda_5 + \eta_6\lambda_6, \qquad (6)$$

where λ_t = combined load condition; λ_1, λ_2, and λ_3 = three basic load conditions; λ_4 and λ_5 = vertical and horizontal seismic loads, respectively; λ_6 = load condition of temperature; η_1, η_2, and η_3 = coefficients of three basic load conditions, respectively, which reflect the contribution of each load condition to the final combination of load conditions; η_4 and η_5 = coefficients of the vertical and horizontal seismic loads; and η_6 = coefficient of the temperature loads.

Twenty-one conditions were analyzed by the FE method, and the allowable stresses method was used to evaluate the performance of structure under different load conditions. Tables 4 and 5 present the envelope values of stress and strip displacements at the midspan of shell under all cases obtained by FE analysis, where $\sigma_{\max}$, $\sigma_{\min}$, δ_x, δ_y, and δ_z represents the maximum stress and minimum stress of elements, and displacements of node at directions x, y, and z regarding all load conditions, respectively. It can be seen that the maximum and minimum values in Tables 4 and 5 varied in a finite range, which suggests that the structure gives a nonuniform distribution of wind load, yet the limited value rarely influenced the performance of structure.

Figure 10 shows the maximum predicted-to-permitted stress ratio (α), which includes the results of all load conditions (q). Regardless of the symmetric structure, the complexity of load conditions applied to the FE model lead to great variation in the ratios. Yet the ratios in Figure 8 illustrates that the maximum stress of members in the structure did not exceed the permission, which means the stiffness and strength of structure perform well under the wind load, and furthermore, the safety of structure was confirmed.

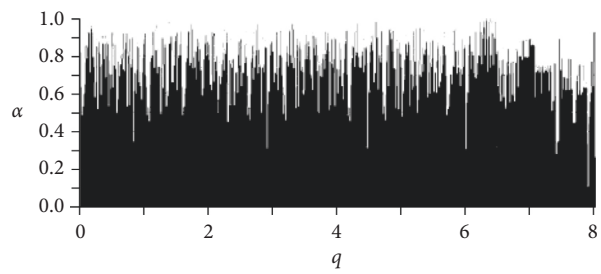

Figure 10: Stress ratio in all load conditions.

5. Conclusions

In this study, wind tunnel tests as well as the numerical simulation of large-span spherical shell roof structure when subjected to different typical wind directions were implemented to investigate its wind pressure characteristics. Wind force coefficients and shape coefficients were obtained to analyze the distribution of wind pressure on the roof structure, and the following conclusions can be summarized:

(1) Both wind force coefficients and shape coefficients change significantly with wind directions, and peak coefficients were obtained at 90°.

(2) For this spherical shell roof, most parts during test were subjected to negative wind pressure, i.e., suction force. Flow separation phenomenon occurred in the windward areas, and accordingly, the maximum negative value was observed at the top of the roof surface. The experimental results proved that the geometry of this spherical shell roof had good mechanical performance.

(3) The dynamic performance of spherical shell roof structure under wind load was studied with numerical method. Twenty-one load cases including the dead loads, live loads, seismic loads, and temperature loads were combined and applied to the FE model. The structure showed a desirable performance under employed load cases, and the stress and displacement of members varied within a permitted range.

Data Availability

No data were used to support this study.

Conflicts of Interest

The authors declared that there are no conflicts of interest.

Acknowledgments

The authors gratefully acknowledge the financial supports for this research by the Natural Science Foundation of China, China (grant no. 51508028), and the Fundamental Research Funds for the Central Universities (grant no. 310828173402).

References

[1] D. P. Billington, *Thin Shell Concrete Structures*, McGraw-Hill, New York, NY, USA, 2nd edition, 1982.

[2] H. C. Noh, "Ultimate strength of large scale reinforced concrete thin shell structures," *Thin-Walled Structures*, vol. 43, no. 9, pp. 1418–1443, 2005.

[3] Z.-T. Chang, M. A. Bradford, and R. I. Gilbert, "Short-term behaviour of shallow thin-walled concrete dome under uniform external pressure," *Thin-Walled Structures*, vol. 49, no. 1, pp. 112–120, 2011.

[4] R. P. Hoxey and A. P. Robertson, "Pressure coefficients for low-rise building envelopes derived from full-scale experiments," *Journal of Wind Engineering and Industrial Aerodynamics*, vol. 53, no. 1-2, pp. 283–297, 1994.

[5] Y. Uematsu, M. Yamada, A. Inoue, and T. Hongo, "Wind loads and wind-induced dynamic behavior of a single-layer latticed dome," *Journal of Wind Engineering and Industrial Aerodynamics*, vol. 66, no. 3, pp. 227–248, 1997.

[6] J. Fu, Q. Zheng, J. Wu, and A. Xu, "Full-scale tests of wind effects on a long span roof structure," *Earthquake Engineering and Engineering Vibration*, vol. 14, no. 2, pp. 361–372, 2015.

[7] Y. Uematsu, T. Moteki, and T. Hongo, "Model of wind pressure field on circular flat roofs and its application to load estimation," *Journal of Wind Engineering and Industrial Aerodynamics*, vol. 96, no. 6-7, pp. 1003–1014, 2008.

[8] Y. Uematsu, K. Watanabe, A. Sasaki, M. Yamada, and T. Hongo, "Wind-induced dynamic response and resultant load estimation of a circular flat roof," *Journal of Wind Engineering and Industrial Aerodynamics*, vol. 83, no. 1–3, pp. 251–261, 1999.

[9] P. Biagini, C. Borri, and L. Facchini, "Wind response of large roofs of stadions and arena," *Journal of Wind Engineering and Industrial Aerodynamics*, vol. 95, no. 9-11, pp. 871–887, 2007.

[10] H. Marukawa, Y. Uematsu, Y. Tamura et al., "Design wind load on a flat long-pan roof," in *Proceedings of the 4th East Asia-acific Conference on Structural Engineering and Construction*, Y. K. Shin, S. P. Chang, and H. M. Koh, Eds., vol. 3, pp. 1619–1624, Seoul, Korea, September 1993.

[11] T. Hongo, *Experimental Study of Wind Forces on Spherical Roofs*, Ph.D. thesis, Tohoku University, Sendai, Japan, 1995.

[12] X. Zhou, Z. Han, M. Gu, A.-A. Zhang, W. Zhang, and W. Fang, "Research on wind-induced responses of a large-scale membrane structure," *Earthquake Engineering and Engineering Vibration*, vol. 12, no. 2, pp. 297–305, 2013.

[13] CS (Chinese Standard) GB 50009-2012, *Load Code for the Design of Building structures*, Ministry of Construction of the People's Republic of China and Quality Supervision Inspection and Quarantine of the People's Republic of China, Beijing, China, 2012, in Chinese.

Hindawi
Mathematical Problems in Engineering
Volume 2019, Article ID 1979275, 13 pages
https://doi.org/10.1155/2019/1979275

Research Article

Dynamic Network Planning of Underground Logistics System on Uncertainty Graph

YiHua Zhong,[1] ShiMing Luo,[1,2] Min Bao,[1] and XiaoDie Lv[1,3]

[1]*School of Science, Southwest Petroleum University, Chengdu, Sichuan 610500, China*
[2]*Neijiang Sixth Middle School, Neijiang, Sichuan 641100, China*
[3]*School of Mathematics and Information Science, Neijiang Normal University, Neijiang, Sichuan 641100, China*

Correspondence should be addressed to YiHua Zhong; zhongyh_65@126.com

Received 15 April 2019; Revised 30 July 2019; Accepted 8 August 2019; Published 23 October 2019

Guest Editor: C. De la O Francisco

When designing the underground logistics system, it is necessary to consider the uncertainty of logistics nodes, high cost, and high risk. This paper employed the theories of uncertain graph and dynamic programming to solve the network planning problem of underground logistics system. Firstly, we proposed the concepts of uncertainty measure matrix and vertices structure uncertainty graph by using uncertainty measure and uncertainty graph. Secondly, vertices structure uncertainty graph of the underground logistics system was constructed based on our proposed vertices structure uncertainty graph and the uncertainty of logistics nodes. Thirdly, the dynamic programming model of the underground logistics system was established, and its solution algorithm was also designed by improving simulated annealing. Finally, the correctness and feasibility of the method was validated by using a numerical example of the underground logistics system in Xianlin district, Nanjing City in China.

1. Introduction

Problems in transportation and logistics had been tackled well since computers and operational research (OR) became available [1]. However, a new challenge to transportation and logistics is the huge pollution and economic impact of transportation on the environment and logistic costs of companies. The underground logistics system (ULS) is the system of underground freight transportation and supply in inner city and among cities. It can reduce urban pollution by using electric energy to achieve transportation of low-carbon environmental protection. Moreover, it can also effectively reduce the cost and traffic pressure on the ground road to alleviate urban traffic congestion. At present, many countries in the world considered developing urban underground logistics system as a new way of alleviating traffic dilemma. Modern underground logistics system has been studied for nearly 30 years. The United States, Britain, Holland, and Japan just only carried out some of the engineering practices for the underground logistics system [2, 3], but there is still not any successful case as an example of studying [4]. Therefore, the international research for ULS is a relatively new expanding field.

The applications of the early ULS are various. American scholars proposed the freight transports by using underground pipeline or tube transport, which were driven by electricity to transport municipal refuse and coal. The Japanese scholars set up an underground mail system between the Tokyo station and the central post office. Holland scholars used the ULS to connect the Aalsmeer flower market, the Schiphol airport, and the Hoofddorp railway transfer station. By using the ULS, timeliness goods such as flowers may be transported in time [5]. But, nowadays the ULS is obviously different from the early transportation system in influence factors of their construction: the city scale and traffic network congestion [6]. The current studies on the ULS mainly focus on three aspects: feasibility analysis, risk assessment, and network planning of logistics system.

Based on the OLS-ASH project (which is used to illustrate the designing of such a highly automated freight transportation system), Pielage proposed and analyzed the

underground freight transport system and its feasibility as well as its specific design steps with the transportation system in Holland [3]. Hane et al. took Tokyo as an example to analyze the influence degree of the cost-benefit of constructing ULS on the original logistics system [7]. In 2004, Qian first presented a new ULS system and studied the traffic congestion of Beijing in China [8]. Chen et al. used macroenvironment to analyze the applicability of the ULS in China's traffic environment and determined the internal and external factors affecting the system. Moreover, the relevant recommendations about risk assessment of building ULS were proposed based on the situation analysis framework [9]. van der Heijden et al. simulated and analyzed the operating characteristics of the underground logistics network structure and the constructing cost and efficiency among different regions [10].

The researches on the node layout and network optimization of the ULS are the hottest research. Johan analyzed and compared the characteristics of different network structures of the ULS, such as punctiform network, linear network, and reticular network [11]. Based on a definite graph whose vertices and edges are predetermined, Zhu et al. established the node location model of 0-1 linear programming to find the best logistics node [12]. Considering the characteristics of urban environment and logistics nodes, Erkayman et al. proposed the fuzzy TOPSIS (technique for order preference by similarity to an ideal solution) method of planning the logistics center [13]. From the point of view of transportation, construction, economy, technology, and sustainable development, Turskis and Zavadskas presented the ARAS-F (fuzzy additive ratio assessment) method to select the logistics center [14]. According to the stage characteristics of integration process on logistics facilities in Beijing, Tianjin, and Hebei, Guo and Zhuang proposed the cloud model to evaluate complex systems [15]. Yan and Qin adopted the bilevel programming model to select the location of the underground logistics nodes, including the upper-level planning model from the perspective of decision-makers and the lower-level planning model from the perspective of customers [16]. Based on plant growth simulation algorithm, Li optimized the network route of ULS in large cities [17]. Binsbergen and Johan studied the optimization method of the route layout in urban underground logistics network [18]. By applying multimodule network analytic hierarchy process (AHP) based on point, linear, and surface, Mu set up a model of set covering to study and analyze the problem of road planning of the ULS [19].

An important premise of the above studies on the ULS is that logistics nodes are predetermined. However, whether a logistics node of an ULS exists or not in real life depends on a number of factors such as total freight volume, transportation cost, traffic congestion index, construction cost, and traffic interruption. Because data and information of expert estimating and judging above those factors have not only fuzziness but also randomness or imprecision in studying the ULS, the above studies only solved the planning of the ULS with determinate logistics nodes. Obviously, it is not very appropriate to formulate the existence of logistics nodes and the edges connecting logistics nodes only by fuzzy theory or random theory. Uncertainty theory proposed in 2007 and refined in 2010 by Liu [20, 21] is a new tool to handle expert data with fuzziness or randomness or imprecision. In 2013, Gao and Gao first introduced uncertainty theory into graph models and proposed a concept of uncertain graph, in which the existence possibility (reliability) of each edge is described by uncertain measures [22]. It is well known that the ULS has the characteristic of high cost and high risk as well as difficulty improving. Moreover, the impact of logistics nodes on the whole system is different. From the view of ULS top-level design, the following problems should be focused: the time order and the evolution process about route construction of its optimal network. Therefore, a technical process for dynamic network planning of the ULS with vertices structure uncertainty graph may be obtained by applying dynamic network programming [23, 24] and extending uncertainty graph proposed by Gao and Gao [22, 23, 25].

In this paper, firstly, the uncertainty graph of logistics nodes will be constructed according to the definition of vertices structure uncertainty graph and the key degree of each logistics node proposed by us. Secondly, the time order of evolution process and dynamic programming model of ULS will be established based on the uncertainty graph of logistics nodes formulated by us. This uncertainty graph of logistics nodes includes the measure size of each logistics node, the measure size of each tunnel, and each network route. Thirdly, the simulated annealing algorithm will be designed to solve this dynamic network optimization model to obtain the evolution process of an ULS construction project. Finally, the optimal construction time order and dynamic evolution process of an ULS will be programmed with an ULS construction project in Xianlin district, Nanjing city, China, by using the method and algorithm proposed in the paper.

The remainder of this paper is organized as follows: in Section 2, uncertainty measures and uncertainty graphs are introduced and formulated. It includes uncertainty measures and the relative definitions of vertices structure uncertainty graph. In Section 3 the vertices structure uncertainty graph based on an uncertainty of logistics nodes is constructed. Section 4 establishes a dynamic programming model of ULS network construction. In Section 5, an algorithm to solve dynamic programming of the ULS based on the simulated annealing algorithm is designed. In Section 6, a numerical case is studied to demonstrate the correctness of concepts and methods proposed in this paper. Section 7 concludes this paper with a brief summary.

2. Uncertainty Measure and Uncertainty Graph

2.1. Uncertainty Measure. Let Γ be a nonempty set and $\mathscr{L}$ be a $\sigma-$ algebra over Γ. Each element Λ in $\mathscr{L}$ is called an event. The set function M is called an uncertain measure if it satisfies the following three axioms [20, 21].

Axiom 1 normality. $M\{\Gamma\} = 1$.

Axiom 2 self-duality. $M\{\Lambda\} + M\{\Lambda^c\} = 1$ for any event Λ.

Axiom 3 subadditivity. For every countable sequence of events $\{\Lambda_i\}_{i=1}^{+\infty}$, we have

$$M\{\cup_{i=1}^{\infty}\Lambda_i\} \leq \sum_{i=1}^{\infty} M\{\Lambda_i\}. \quad (1)$$

The triplet (Γ, L, M) is called an uncertainty space. Uncertainty measure is interpreted as the personal belief degree (not frequency) of an uncertain event that may happen. Thus, uncertainty measure and belief degree are synonymous. Uncertainty measure depends on the personal knowledge concerning the event. It will change if the state of knowledge changes. In other words, it may be understood simply as a probability Pr in a random environment, or a credibility measure Cr in the fuzzy environment, or a trust value Tr in the rough environment.

2.2. Vertices Structure Uncertainty Graph. The definition of an uncertain graph was first proposed by Gao and Gao [22] in 2013. But their definition assumed that the vertices in the graph are predetermined. Therefore, their definition may be considered as only applying to a special uncertain graph whose edges are not predetermined and whose existence possibility (reliability) of each edge is described by uncertain measures. It is called as the edge structure uncertainty graph by us. By analogy of its definition and the idea of adjacent matrix representing graph, we present definitions of uncertainty measure matrix and vertices structure uncertainty graph as follows.

Definition 1. The graph with uncertain vertices structure uniquely corresponds to an uncertainty measure matrix $\Phi = (\phi_{ij})_{n\times n}$ if and only if ϕ_{ij} satisfies the following:

(1) When $i = j$, $\phi_{ii} = M\{v_i = 1\}$ represents the uncertainty measure of vertex v_i existence, which is simply denoted as ϕ_i

(2) When $i \neq j$, $\phi_{ij} = M\{v_i v_j = 1\}$ represents the uncertainty measure of the edge connecting vertex v_i and vertex v_j

where $v_i = 1$ indicates that vertex i exists, $v_i = 0$ indicates that vertex i does not exist, $v_i v_j = 1$ indicates that the edge connecting vertices i and j exists, and $v_i v_j = 0$ indicates that the edge connecting vertices i and j does not exist.

Based on the uncertainty measure matrix and the definition of the edge structure uncertainty graph, we propose a definition of the vertices structure uncertainty graph as follows.

Definition 2. The graph with uncertain vertices structure is a three triple which can be denoted as $\mathcal{N} = (V, E, \Phi)$. V is the vertex set, and E is the edge set. Φ is the uncertainty measure matrix corresponding to an uncertain graph. It is simply called as a vertices structure uncertainty graph, where V and E determine the structure of the uncertain graph, and the uncertainty measure matrix Φ shows measures of vertices existing and measures of edges existing to connect these uncertain vertices in the graph.

For more intuitively understanding the edge structure uncertainty graph and the vertices structure uncertainty graph, Figure 1 gives a simple uncertain graph for vertices A, B, and C and edges AB, AC, and BC.

In Figure 1(a), if vertex O exists in an uncertainty measure M, then edges OA, OB, and OC must exist with uncertainty measures. Assuming that the edges OA, OB, and OC exist with the uncertainty measures M_a, M_b, and M_c, respectively, and $0 \leq M_a, M_b, M_c, M \leq 1$, then the uncertainty measure matrix corresponding to this graph satisfies the following:

$$\Phi = \begin{pmatrix} 1 & 1 & 1 & M_a \\ 1 & 1 & 1 & M_b \\ 1 & 1 & 1 & M_c \\ M_a & M_b & M_c & M \end{pmatrix}. \quad (2)$$

In Figure 1(b), if vertex O exists (that is, $M = 1$), but edges OA, OB, and OC exist with uncertainty measures M_a, M_b, and M_c, respectively, then the uncertainty measure matrix corresponding to this graph satisfies the following:

$$\Phi = \begin{pmatrix} 1 & 1 & 1 & M_a \\ 1 & 1 & 1 & M_b \\ 1 & 1 & 1 & M_c \\ M_a & M_b & M_c & 1 \end{pmatrix}. \quad (3)$$

If vertex O does not exist (that is, $M = 0$), then edges OA, OB, and OC must not exist, and then the uncertainty measure matrix corresponding to this graph satisfies the following:

$$\Phi = \begin{pmatrix} 1 & 1 & 1 & 0 \\ 1 & 1 & 1 & 0 \\ 1 & 1 & 1 & 0 \\ 0 & 0 & 0 & 0 \end{pmatrix}. \quad (4)$$

Comparing the above three uncertainty measure matrices (2)–(4), we observe that matrices (3) and (4) are the special cases of matrix (2). Thus, the concept of vertices structure uncertainty graph proposed by us extends the concepts of the existing graphs, which may depict the concepts such as graph, probability graph, fuzzy graph, and uncertain graph.

3. Vertices Structure Uncertainty Graph Based on the Uncertainty of Logistics Nodes

3.1. Uncertainty Measure on the Existence of Logistics Nodes. When designing an ULS, the construction of logistics nodes on an area usually adopts location planning to make a preliminary determination [11–18]. The ULS has the characteristics of high cost and high risk as well as difficult improving. Especially, the impact of each logistics node on the whole logistics system is different. Thus, it is necessary to

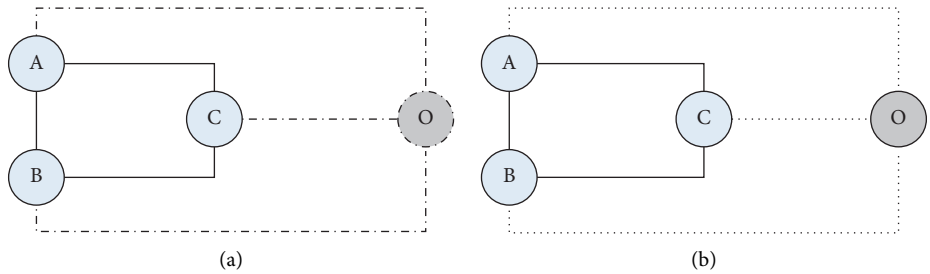

Figure 1: Two uncertain graphs with uncertain structure. (a) The vertex O exists in a measure. (b) The vertex O must exist and OA, OB, and OC must exist with a measure.

analyze and compute the key degree of each logistics node in the dynamic programming of an ULS network.

Let there be n alternative logistics nodes in an ULS. Based on the impact degree of no-constructing logistics node i on the whole logistics network, we present using the impact degree to depict the key degree of logistics node i. Let U_0 be the cost index of all logistics nodes operating normally (no interruption) and U_i be the cost index of the ith logistics node interrupting. The cost here could be the total freight volume, transportation cost, traffic congestion index, or construction cost of the ULS network. Thus, the key degree M_i of the ith logistics node may be computed by using the following formula:

$$M_i = \frac{|U_i - U_0|}{U_0}, \tag{5}$$

where $M_i = 0$ $(U_i = U_0,\ i \in \{1, 2, \ldots, n\})$ means that the interruption of the ith logistics node has no effect on the whole network; that is, the ith logistics node is not important in the whole network. The bigger the M_i is, the more critical the ith logistics node is.

From the point of view of graph theory, the key degree of each logistics node decides the possibility of the corresponding vertex (logistics node) existence in the ULS. That is, the uncertainty measure of vertex existence is different.

The bigger the key degree is, the bigger the possibility of the vertex existence is, and vice versa. By standardization key degree M_i, the ith vertex uncertainty measure can be obtained according to the following formula:

$$\phi_i = \frac{M_i - \min_{i\in\{1,2,\ldots,n\}}\{M_i\}}{\max_{i\in\{1,2,\ldots,n\}}\{M_i\} - \min_{i\in\{1,2,\ldots,n\}}\{M_i\}} \times 100\%. \tag{6}$$

3.2. Uncertainty Measure of the Edge Connecting Two Logistics Nodes. In an ULS network, if a logistics node does not exist, then the edges connecting it must not exist. According to this phenomenon, the uncertainty of an edge (route) may be depicted by using the freight volume.

If h_{ij} represents the freight volume of from logistics node i to logistics node j, then the uncertainty measure of the edge connecting vertices i and j may defined as follows:

$$\phi_{ij} = \frac{h_{ij} - \min_{i,j\in\{1,2,\cdots,n\}}\{h_{ij}\}}{\max_{i,j\in\{1,2,\ldots,n\}}\{h_{ij}\} - \min_{i,j\in\{1,2,\ldots,n\}}\{h_{ij}\}} \times 100\%. \tag{7}$$

3.3. Vertices Structure Uncertainty Graph. According to definition 2 and Sections 3.1 and 3.2, an ULS network may model as an uncertainty graph $\mathcal{N} = (V, E, \Phi)$. In which, logistics node i is taken as vertex v_i $(i \in \{1, 2, \ldots, n\})$ of the graph, where n is the total number of logistics nodes, and the vertex set is denoted as $V = \{v_1, v_2, \ldots, v_n\}$; the transportation road (or tunnel) between vertex v_i and vertex v_j is taken as an edge e_k $(k \in \{1, 2, \ldots, m\})$ of the graph, where m is the total number of edges of the graph, and the edge set of the graph is denoted as $E = \{e_1, e_2, \ldots, e_m\}$; uncertainty measure matrix $\Phi = (\phi_{ij})_{n\times n}$, when $i = j$, $\phi_{ii} = \phi_i$, and it may be computed by using formula (6); when $i \neq j$, ϕ_{ij} may be computed by using formula (7). Thus, a schematic diagram on logistics nodes of vertices structure uncertainty graph is shown in Figure 2.

In Figure 2, numbers on vertices and edges represent uncertainty measures for logistics nodes and transportation roads (or tunnels) in the ULS, which can be calculated by using formulas (6) and (7), respectively. The number 1.0 at vertices B, E, and D means that the effects of logistics nodes B, E, and D on the cost index of ULS are the same. Moreover, their effects are the greatest among the effects of logistics nodes on the cost index of the ULS. Therefore, logistics nodes B, E, and D must exist in the vertices structure uncertainty graph of the ULS. The numbers 0.5 and 0.7 at nodes A and C mean that they are less important than nodes B, E, and D, and the possibilities of their existing in the vertices structure uncertainty graph of ULS are 0.5 and 0.7, respectively. The numbers 0.7, 0.2, and 0.3 on edges BA, AC, and BC mean that the possibilities of building transport roads (or tunnels) BA, AC, and BC between nodes B, A, and C are 0.7, 0.2, and 0.3, respectively; the number 1.0 on edges BE and DB means that transport roads (or tunnels) BE and DB must be built between nodes B, D, and E, while the number 0.4 on edge DE means that the possibility of building transport road (or tunnel) DE between nodes D and E is only 0.4.

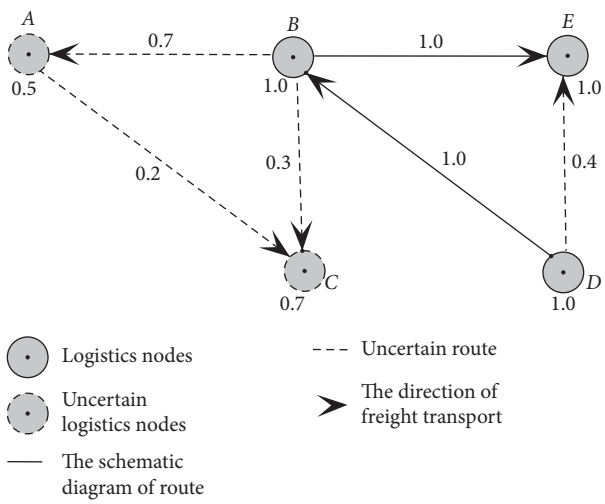

Figure 2: Schematic diagram on logistics nodes of vertices structure uncertainty graph.

4. Dynamic Programming Model of ULS Network Construction

In view of the above analysis in Section 3, we may establish a dynamic programming model of the ULS network construction to obtain its schedule and dynamic evolution process. Let an ULS have n logistics nodes and m tunnels. Then, it may model as an uncertainty graph with n vertices and m edges based on the vertices structure uncertainty graph. During the process of construction, it usually needs to be completed in r years. If the total route length of the ULS is D_{total}, then the tunnel (route) length to be built in every year is $D_{\text{wish}} = D_{\text{total}}/r$. Therefore, construction process in a year may be analyzed as follows:

(1) Number the logistic nodes according to the decreasing order of their uncertainty measures ϕ_i, $i = 1, 2, \ldots, n$

(2) Schedule the ULS network routes to be constructed in the order of $1, 2, \ldots, m$ based on the vertices structure uncertainty graph; that is, the ULS network has m edges

(3) Establish dynamic programming model

4.1. Set Variables. Let a route be built at each stage. Then, we may set the following variables:

k: stage variable $k \in \{1, 2, \ldots, m\}$.

d_k: the length of the kth route, as the distance of edge BC is 5 km in Figure 3.

c_k: the value of the kth route connecting vertices v_i and v_j; that is, the uncertain measure ϕ_{ij} of edge e_k existing, as an example $c_k = 0.3$ means the uncertain measure of edge BC existing in Figure 3.

S_{k+1}: the total length of previous k routes (tunnels) allowed to be constructed in the ULS network at the beginning of the kth stage, where $S_1 = 0$.

x_k: whether the kth route is built or not, where $x_k = 0$ means that it is not built and $x_k = 1$ means that it is built.

4.2. State Transfer Functions. Because the total length of previous $k-1$ routes (tunnels) allowed to be constructed before the kth stage is S_k, the length of the tunnel constructed in the kth stage is $d_k \cdot x_k$, and the total length of previous k routes (tunnels) allowed to be constructed in the ULS network at the beginning of the kth stage $S_{k+1} = S_k + d_k \cdot x_k$. Then, the state transfer equation of the total length of the tunnel allowed to be constructed is as follows:

$$S_k = S_{k+1} - d_k \cdot x_k, \quad k = 1, 2, \ldots, m. \tag{8}$$

A graphic description that graphically explains what different variables represent can be seen in Figure 3. Figure 3(a) shows that the total length of a tunnel allowed to be constructed before the beginning of stage 1 is $S_1 = 0$. The length of tunnel BD constructed in the first stage is 7, so the total length of previous 1 tunnel allowed to be constructed at the beginning of the first stage is $S_2 = S_1 + d_1 \cdot x_1 = 0 + 7 \times 1 = 7$. Figure 3(b) shows that the length of a tunnel allowed to be constructed before the beginning of stage 2 is $S_2 = 7$. The length of tunnel BE constructed in the second stage is 6, so the total length of previous 2 tunnels allowed to be constructed at the beginning of the second stage is $S_3 = S_2 + d_2 \cdot x_2 = 7 + 6 \times 1 = 13$.

4.3. Fundamental Equation. Assuming that $f_k(S_{k+1})$ represents the maximum value that the total length of being allowed construction routes is less than S_{k+1}, only previous k routes are built by optimal strategy. Then, the sequential recursion relation is as follows:

$$\begin{cases} f_k(S_{k+1}) = \max\limits_{0 \le d_k x_k \le S_{k+1}} \{c_k x_k + f_{k-1}(S_{k+1} - d_k x_k)\}, \\ \qquad\qquad\qquad\qquad\qquad\qquad k = 1, 2, \ldots, m, \\ f_0(S_1) = 0. \end{cases} \tag{9}$$

For more easy calculation, equation (9) is transformed into the following recursion relation formula:

$$\begin{cases} f_k(S_{k+1}) = \max\limits_{0 \le x_k \le \left[S_{k+1}/d_{e_k}\right]} \{c_k x_k + f_{k-1}(S_{k+1} - d_k x_k)\}, \\ \qquad\qquad\qquad\qquad\qquad\qquad k = 1, 2, \ldots, m, \\ f_0(S_1) = 0. \end{cases} \tag{10}$$

Through calculating by the recursion relation equation (10) in sequence, the optimal result of construction routes can be obtained.

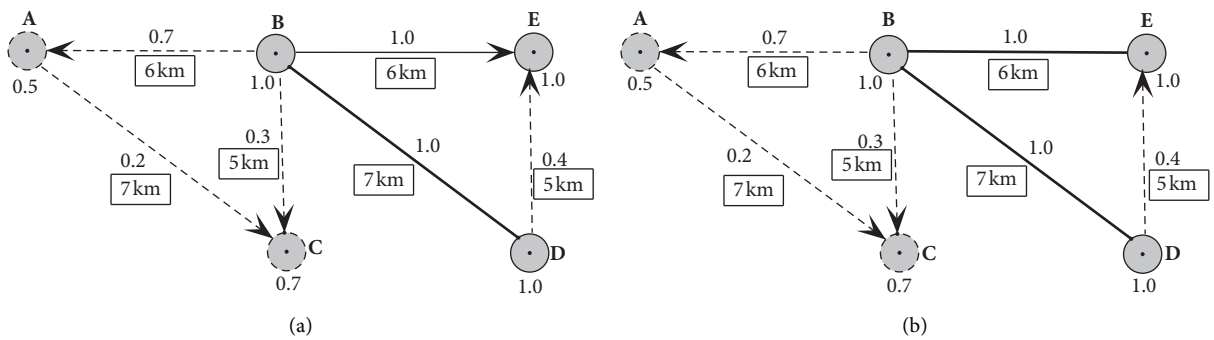

Figure 3: A graphic description that graphically explains what different variables represent.

5. A Dynamic Programming Algorithm for ULS Construction Based on Simulated Annealing Algorithm

The idea of original simulated annealing (SA) algorithm comes from the physical annealing process [19, 26]. It is often used to solve the problem of combinatorial optimization. Obviously, the problem of ULS construction planning is a combinatorial optimization problem with uncertain measures based on Section 4. Therefore, we present an improving SA to solve the problem of ULS construction project.

5.1. The Idea of Improving SA Algorithm. The idea is first to compute the uncertainty measures on logistics nodes and transportation roads (tunnels) connecting logistics nodes to establish the network road of ULS with the vertices structure uncertainty graph and then to use solid annealing to simulate the combinatorial optimization problem [27, 28], which is as follows.

Firstly, according to the cost index of each logistics node and the existing freight volume in logistics system, the uncertainty measures of logistics nodes and transportation roads (tunnels) between logistics nodes are computed. Based on these, the network road of the ULS with the vertices structure uncertainty graph is established.

Then, in order to get the transportation road (tunnel) construction process, priority should be given to the establishment of key logistics nodes and key tunnels associated with key logistics nodes on the basis of the different degrees of impact of each node on the whole logistics system and the different demands of freight volume on each transportation road (tunnel).

Secondly, when the critical degree of logistics nodes is the same, priority should be given to the construction of transportation roads (tunnels) with larger freight volume.

Comparing it with the original simulated annealing algorithm, the differences lie in the process of judging the generation and acceptance of new solutions. Firstly, the uncertainty measures of vertices and edges are calculated, and the edges associated with the vertices having larger uncertainty measures are selected as candidate sets. Then, the uncertainty measures on the edges of candidate sets are judged. Secondly, in simulating internal energy E, the computation of E being taken as objective function value f, the value (freight volume) of the tunnels needs to be first calculated as the uncertain measures ϕ_{ij} of the network roads of the ULS.

5.2. The Steps of Improving SA Algorithm. On the basis of the above idea and the algorithm of original SA, the concrete steps of the improving SA algorithm are as follows:

Step 1: compute the uncertainty measures on logistics nodes and transportation roads (tunnels) connecting logistics nodes of the ULS with the vertices structure uncertainty graph.

Step 2: number the logistic nodes according to the decreasing order of their uncertainty measures ϕ_i, $i = 1, 2, \ldots, n$.

Step 3: schedule the ULS network routes to be constructed in the order of $k = 1, 2, \ldots, m$ based on the decreasing order of their uncertainty measures ϕ_{ij} of the existing edge e_k.

Step 4: determine the solution space $S = \{x_1, x_2, \ldots, x_m \mid \sum_{k=1}^{m} d_k x_k < D_{\text{wish}}\}$, where each feasible solution is represented by using a binary string.

Step 5: determine the internal energy E. The internal energy E is depicted as the objective function value f—the value (freight volume) of the tunnels; i.e., $E = f(x_1, x_2, \ldots, x_m) = \sum_{k=1}^{m} c_k x_k$, $c_k = \phi_{ij}$.

Step 6: let the initial temperature t and initial solution $x = x_0$.

Step 7: generate a new solution x_t. A route edge (tunnel) x is first selected randomly. If it is not in the ULS that has been constructed, then it will allow to be constructed as a new solution $x = x_t$. Otherwise, the next tunnel of x is chosen randomly as the edge x_t; that is, a new solution is generated by choosing x_t in the neighborhood of x.

Step 8: internal circulation.

(1) Calculate objective function values E corresponding to x and x_t. If the objective function value of x_t is less than that of x, then stop and let $x = x_t$.

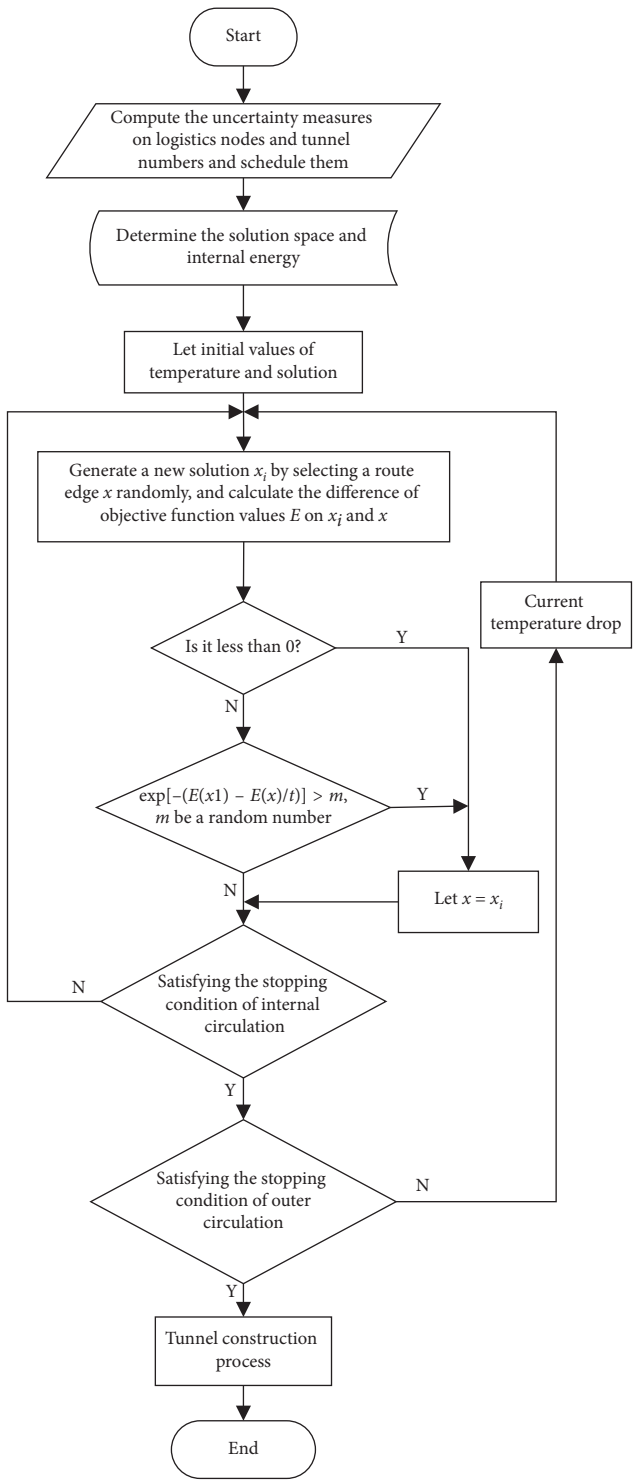

Figure 4: The flow diagram of the improving SA algorithm.

Otherwise, if $\exp[-(E(x_t) - E(x))/t] > \varepsilon$, where $\varepsilon \in (0, 1)$ is a random number, then stop and let $x = x_t$.

(2) When the stop condition in (1) is not satisfied, then update t and repeat (1).

Step 9: external circulation.

(1) Cool down according to equations (11)–(13).

(2) If the stop condition of external circulation is not satisfied, then go to Step 5. Otherwise, stop the algorithm, where the value difference Δf and the length difference Δd in the edge of planning to be built tunnel in the ULS are satisfied, respectively:

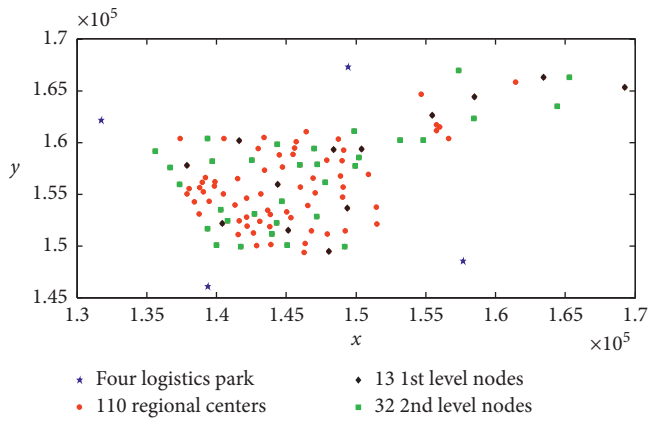

Figure 5: Position distribution of logistics nodes at all levels in Xianlin district.

Table 1: The related data of logistics nodes.

Number	X position	Y position	Inflow	Outflow
1	148037.4	149443.9	1544.086	1528.184
2	145146.8	151489.6	11698.71	11064.55
3	140416.6	152146.1	14112.56	14103.54
4	149366.9	153648.1	9541.856	9226.744
5	144403.3	155930	10114.65	12104.62
6	137889.7	157781.7	8299.6	8540.79
7	141629.7	160163.7	6707.157	5996.62
8	148375.7	159294.3	7146.025	6914.614
9	150413.2	159364.7	10813.93	9715.012
10	155477.4	162651.1	6601.267	5761.77
11	158487.3	164413.4	6442.007	5625.619
12	169251.1	165333.2	153.939	252.769
13	163428	166293.4	6622.373	6225.333
14	141732.2	149908	2826.742	2689.738
15	145062.7	150092.6	2546.253	2431.514
16	139998.8	150082.7	2334.953	2429.127
17	149198.5	149918.9	2129.194	2057.143
18	143976.3	151159.2	1634.509	1524.001
19	144302.1	152239.5	964.361	865.667
20	140808.2	152432.5	3241.555	3426.522
21	139366.7	151652.6	2525.864	2662.456
22	142733.4	153099.6	2782.18	2505.738
23	147188.8	152823.2	4208.429	4041.365
24	140309.2	153473.8	2993.329	2710.818
25	144691	154317	2317.39	2754.09
26	147771.4	156163	2351.513	2176.283
27	149951.9	157738.3	4753.68	4090.284
28	137348.1	155938.5	4021.458	3672.704
29	136656.2	157553.6	1751.44	1809.175
30	139713.8	158198.1	2784.112	2434.092
31	142527.8	158313	3553.178	2896.085
32	135607.1	159148.9	1088.694	1851.249
33	144348.9	159828.8	987.691	966.32
34	139356.9	160405.2	2285.787	2269.248
35	145961.8	157814.7	1255.392	1330.97
36	147221.1	157904.4	3301.446	2454.303
37	150211.9	158547.6	4969.057	4677.888
38	146987.7	159418.2	4904.498	4855.147
39	149877.2	161091	859.515	884.769
40	154830.1	160255.1	4260.346	3322.93
41	153147	160216.5	2080.225	1882.86
42	164429.9	163490	2661.528	1977.437
43	158431.3	162322.4	2955.537	2692.746
44	165296	166307.5	967.672	1021.723
45	157354.7	166956.7	2378.161	1880.603

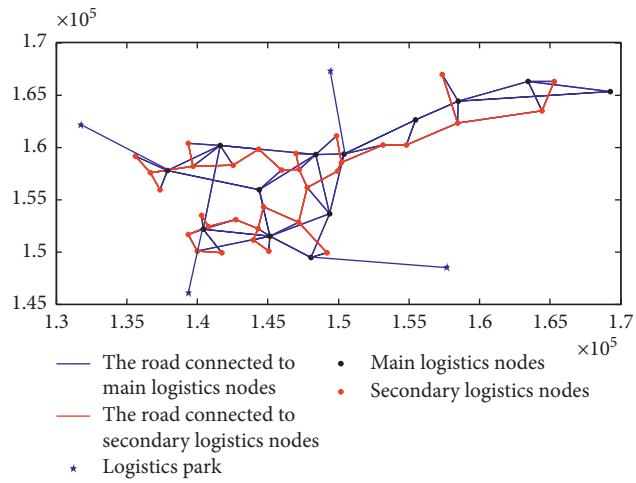

Figure 6: The network road of ULS.

$$\Delta f = \begin{cases} c_i, & \text{constructing the } i\text{th tunnel during the period,} \\ c_i - c_j, & \text{constructing the } i\text{th tunnel and not constructing the } j\text{th tunnel in the period,} \\ c_j - c_i, & \text{constructing the } j\text{th tunnel and not constructing the } i\text{th tunnel during the period,} \end{cases} \tag{11}$$

$$\Delta d = \begin{cases} d_i, & \text{constructing the } i\text{th tunnel during the period,} \\ d_i - d_j, & \text{constructing the } i\text{th tunnel and not constructing the } j\text{th tunnel in the period,} \\ d_j - d_i, & \text{constructing the } j\text{th tunnel and not constructing the } i\text{th tunnel during the period,} \end{cases} \tag{12}$$

$$p = \begin{cases} 0, & \text{if } d + \Delta d > D_{\text{wish}}, \\ 1, & \text{if } d + \Delta d \le D_{\text{wish}}, \text{ and } \Delta f > 0, \\ \exp(\Delta f / t_k), & \text{otherwise,} \end{cases} \tag{13}$$

Δd is the mileage increment of the total length of constructing the tunnels in the current planning. When planning to construct the tunnels, it is not known whether the tunnel will be built or not. Therefore, the extended metropolis criterion rule is used to compute p: where t_k is the temperature control parameter.

5.3. The Flow Diagram of Improving SA Algorithm. The flow diagram of the improving SA algorithms can be seen in Figure 4.

6. Case Study

6.1. Problem. The ULS dynamic network programming method proposed in this paper is used to plan the optimal schedule of network route construction in Xianlin district, Nanjing city, based on the underground logistics system (ULS) mentioned in question F of the 14th "Huawei cup" China Postgraduate Mathematic Contest in Modelling in 2017. The network construction project of underground logistics system requires constructing 45 logistics nodes (the numbers 1–13 are the 1st level nodes; the numbers 14–45 are the 2nd level nodes) and 81 tunnels (the total length is 290 km) during the 8th year. Figure 5 shows position distribution of logistics nodes at all levels; Table 1 gives the related data of the nodes and tunnels on the ULS.

6.2. The Uncertainty Graph on Logistics Nodes. Using the method of formulating the vertices structure uncertainty graph based on the uncertainty of logistics nodes in Section 3, the network road of the ULS with the vertices structure uncertainty graph is as shown in Figure 6.

6.3. The Construction Schedule and Dynamic Evolution Process of ULS Network Route. Based on the methods in Sections 4 and 5, let parameters of the improving SA algorithm be as follows: cutoff temperature TF = 0.000001, annealing factor $a = 0.9$, initial temperature $T = 100$, and iterations res = 8100. By using the improving SA, we obtained the total number of tunnels to plan to be built and the corresponding serial numbers of tunnels, the actual total length network to plan to be completed, and the total freight volume in each year during 8 years, which can be seen in Table 2. Table 2 shows that the total length to be established in every year is roughly the same. The tunnel with bigger uncertainty measure of

Table 2: The relevant data tables for the tunnel construction in each year.

	Total flow of freight transport	Total length of tunnels	Total number of tunnels	The number of constructed tunnels
First year	302.476	39.468	19	2, 5, 6, 25, 27, 29, 32, 35, 54, 60, 61, 64, 65, 68, 69, 71, 73, 75, 44
Second year	288.073	36.332	10	7, 13, 17, 22, 23, 38, 40, 47, 50, 81
Third year	110.929	36.550	10	1, 9, 11, 14, 20, 21, 24, 31, 37, 43
Fourth year	115.789	36.371	10	3, 4, 12, 15, 26, 30, 33, 36, 41, 45
Fifth year	121.275	36.829	9	8, 10, 19, 49, 52, 56, 53, 57, 59
Sixth year	127.338	35.346	7	16, 28, 42, 46, 77, 79, 80
Seventh year	133.705	36.967	9	18, 34, 39, 48, 51, 62, 63, 66, 67
Eighth year	144.786	32.137	7	55, 58, 70, 72, 74, 76, 78
Total	1344.371	290	81	

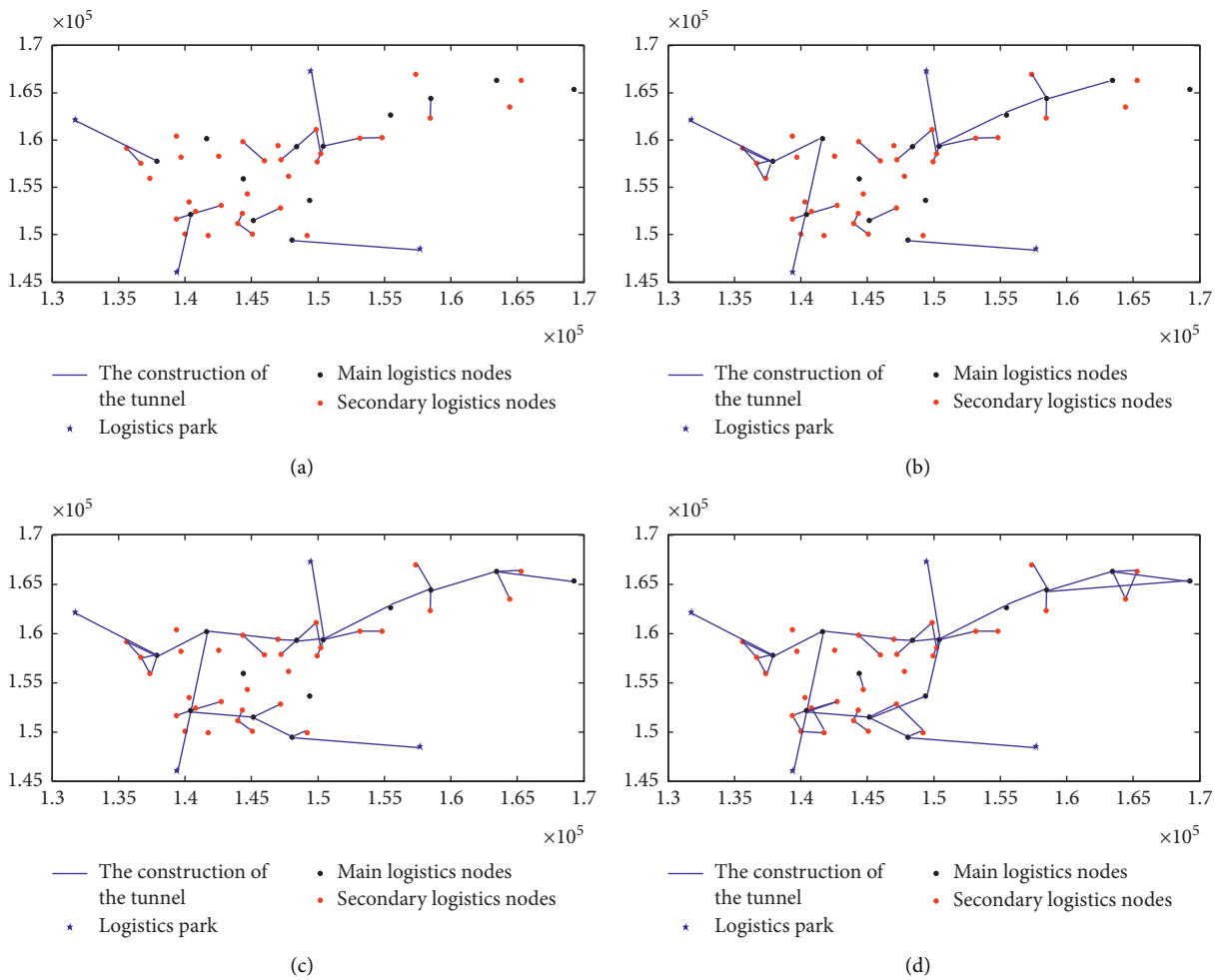

Figure 7: Continued.

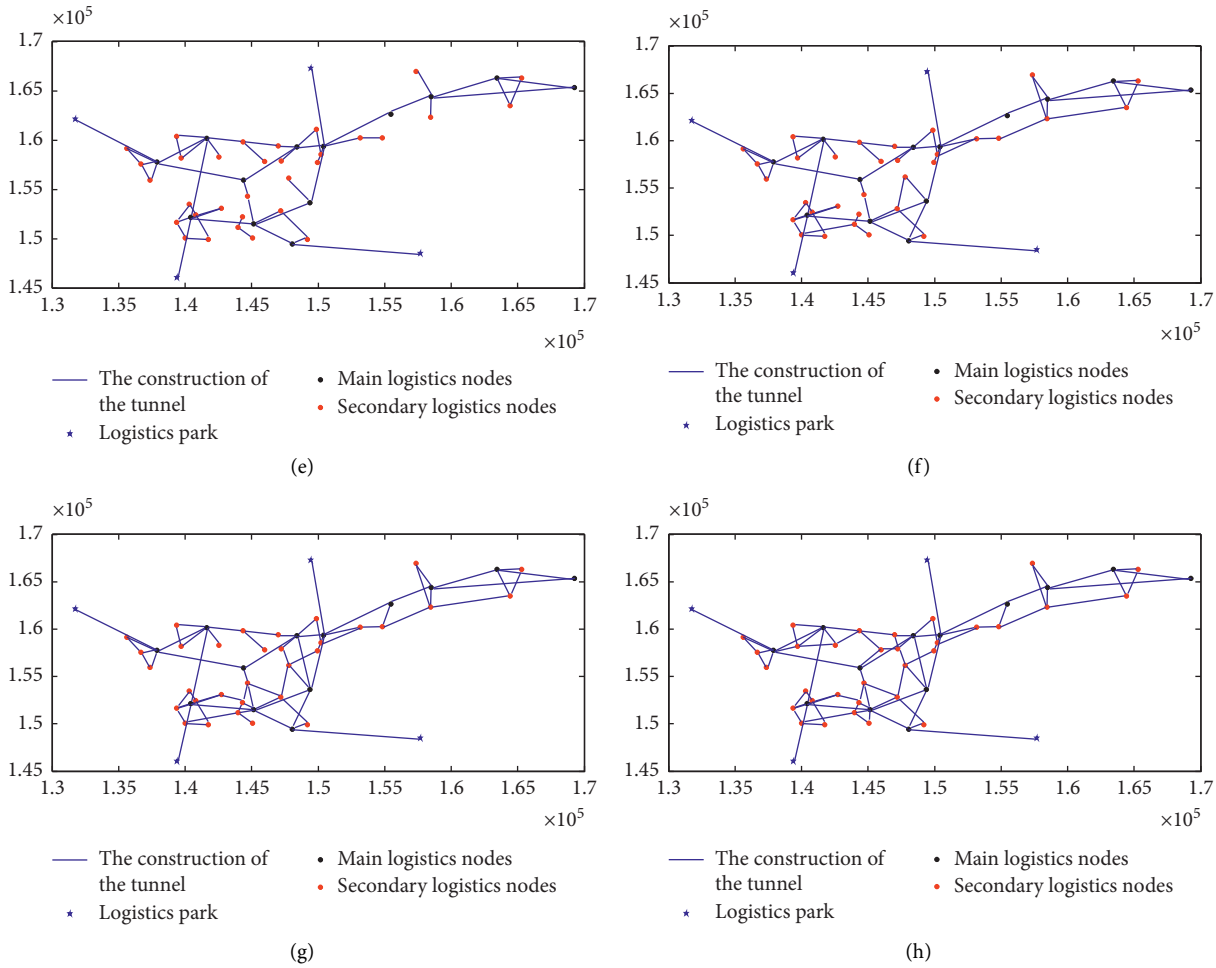

Figure 7: The evolution process of ULS construction. (a) First year. (b) Second year. (c) Third year. (d) Fourth year. (e) Fifth year. (f) Sixth year. (g) Seventh year. (h) Eighth year.

logistics nodes existing is always constructed in priority. That is, the relevant logistics nodes and tunnels with larger total freight volume are constructed in priority during the previous two years.

In addition, Figure 7 gives the evolution process of the whole underground logistics network construction in this district. That is, it gives a schedule chart of tunnel construction that is actually built each year in 8 years.

It can be seen from Figure 7 that the network built in every year is a block except the first year. It is because that the freight volume of each logistics node is also relatively large around the logistics node with large freight volume. Although the construction network in the first year seems to be scattered, it was found that most of the tunnels built in the first year are connected with the key logistics nodes. Because the key degree (the freight volume) is relatively large at the key logistics nodes, the key nodes should be given priority in the top layer design.

7. Conclusion

For the ULS being a new type of efficient transportation system, the route construction planning of the ULS network is essentially a key step of constructing ULS. Because the dynamic network planning of the ULS is a complex problem, we used comprehensively the graph theory, optimization theory, uncertain programming, dynamic optimization model, and simulated annealing algorithm to study it. After the relevant information of ground freight traffic is available, firstly, the influence degree of a logistics node interruption on the whole logistics network is used to depict the key degree of the logistics node, and it formulates the uncertainty measure of the logistics node. For the bigger the freight volume is, the bigger the possibility of the edge existence is; thus, the freight volume is used to express the uncertainty measure of edge connecting two logistics nodes. Secondly, a vertices structure uncertainty graph is formulated. Finally, a dynamic programming model of the ULS network construction is made, and an improving simulated annealing algorithm is designed to solve dynamic network optimization and the schedule problem of the ULS construction. The optimal time process of the network route construction in Xianlin district, Nanjing, China, shows that the ideas and methods proposed in this paper are correct and feasible. The established programming model and the design algorithm are effective and reliable for solving the network optimization of the ULS.

About the route construction planning of the ULS network, we only study its dynamic network programming of the ULS with uncertain logistics nodes. It has still many problems worth studying, such as uncertain programming model of its route based on expected-value model, chance-constrained programming, and dependent-chance programming; network layout based on linear graph, ring graph, and grid graph; and its programming problem of considering more comprehensive uncertainty factor.

Data Availability

The data used to support the findings of this study are available from the corresponding author upon request.

Conflicts of Interest

The authors declare that they have no conflicts of interest.

Acknowledgments

This work was supported by the Double First-Rate Higher School Construction Foundation of Sichuan Finance Department and Education Department (Grant no. 2050205).

References

[1] M. G. Speranza, "Trends in transportation and logistics," *European Journal of Operational Research*, vol. 264, no. 3, pp. 830–836, 2018.

[2] O. N. Egbunike and A. T. Potter, "Are freight pipelines a pipe dream? A critical review of the UK and European perspective," *Journal of Transport Geography*, vol. 19, no. 4, pp. 499–508, 2011.

[3] B. J. Pielage, "Underground freight transportation. A new development for automated freight transportation systems in the Netherlands," in *Proceedings of the IEEE Intelligent Transportation Systems*, pp. 762–767, Oakland, CA, USA, August 2001.

[4] I. E. Zevgolis, A. A. Mavrikos, and D. C. Kaliampakos, "Construction, storage capacity and economics of an underground warehousing-logistics center in Athens, Greece," *Tunnelling and Underground Space Technology*, vol. 19, no. 2, pp. 165–173, 2004.

[5] N. Rezaie, A. Tabesh, M. Najafi, B. Ma, and S. H. Mousavipour, "Evaluation of applications and the comparison of routes for underground freight transportation in Texas," in *Proceedings of the Pipelines 2016*, pp. 847–856, Kansas City, MO, USA, July 2016.

[6] E. Kulińska and M. Odlanicka-Poczobutt, "Facilitation of urban transport through a pipeline supply network," *Transportation Research Procedia*, vol. 16, pp. 255–265, 2016.

[7] K. Hane, K. Okutsu, N. Matsui, and S. Kosugi, "Applicability of pneumatic capsule pipeline to radioactive waste disposal facility," *New Pipeline Technologies, Security&Safety*, vol. 36, pp. 1615–1624, 2003.

[8] Q. H. Qian, "Construction of underground expressway and underground logistics system in mega cities-a new idea for solving traffic problems in China's megacities," *Science and Technology Review*, vol. 4, no. 4, pp. 3–6, 2004.

[9] Z. Chen, J. Dong, and R. Ren, "Urban underground logistics system in China: opportunities or challenges?," *Underground Space*, vol. 2, no. 3, 2017.

[10] M. C. van der Heijden, A. V. Harten, M. J. R. Ebben, Y. A. Saanen, E. C. Valentin, and A. Verbraeck, "Using simulation to design all automated underground system for transporting freight around Schiphol airport," *Interfaces*, vol. 32, no. 4, pp. 1–19, 2002.

[11] V. Johan, "Underground logistics systems for goods distribution in urban areas: overview and experience in the Netherlands," in *Proccedings of the ISUFT 2005*, Shanghai, China, 2005.

[12] J. Zhu, K. Huang, Y. Pu, and J. Zhang, "Research on optimization model for urban underground logistics system," in *Proccedings of the International Conference on Transportation Engineering*, pp. 4192–4197, Chengdu, China, July 2007.

[13] B. Erkayman, E. Gundogar, G. Akkaya, and M. Ipek, "A fuzzy TOPSIS approach for logistics center location problem," *Journal of Business Case Studies (JBCS)*, vol. 7, no. 3, pp. 49–54, 2011.

[14] Z. Turskis and E. K. Zavadskas, "A new fuzzy additive ratio assessment method (ARAS-F). Case study: the analysis of fuzzy multiple criteria in order to select the logistic centers location," *Transport*, vol. 25, no. 4, pp. 423–432, 2010.

[15] Q. Guo and J. Zhuang, "Measuring the integration level of logistics facilities in Beijing-Tianjin-Hebei based on cloud model," *China Business and Market*, vol. 32, no. 1, pp. 113–121, 2018.

[16] W. T. Yan and Y. H. Qin, "Research on bi-level programming model and algorithm of underground logistics node location," *Chinese Journal of Underground Space and Engineering*, vol. 12, no. 4, pp. 870–874, 2016.

[17] Q. Q. Li, *Optimization Layout of Underground Logistics Network in Big Cities with Plant Growth Simulation Algorithm*, Hangzhou Dianzi University, Hangzhou, China, 2013.

[18] V. A. J. Binsbergen and V. Johan, *Innovation Steps towards Efficient Goods Distribution Systems for Urban Areas*, Delft University of Technology, Delft, The Netherlands, 2001.

[19] S. L. Mu, *The Research of Route Planning of Urban Underground Logistics System Based on Beijing*, Shijiazhuang TieDao University, Shaoxing, China, 2015.

[20] B. Liu, *Uncertainty Theory*, Springer-Verlag, Berlin, Germany, 2nd edition, 2007.

[21] B. Liu, *Uncertainty Theory: A Branch of Mathematics for Modeling Human Uncertainty*, Springer-Verlag, Berlin, Germany, 2010.

[22] X. Gao and Y. Gao, "Connectedness index of uncertain graph," *International Journal of Uncertainty, Fuzziness and Knowledge-Based Systems*, vol. 21, no. 1, pp. 127–137, 2013.

[23] Y. Gao, "Uncertain models for single facility location problems on networks," *Applied Mathematical Modelling*, vol. 36, no. 6, pp. 2592–2599, 2012.

[24] C. K. Ting, S. T. Li, and C. N. Lee, "TGA: a new integrated approach to evolutionary algorithms," *IEEE Congress on Evolutionary Computation*, vol. 2, no. 2, pp. 917–924, 2001.

[25] Y. Gao, "Analysis of k-out-of-n system with uncertain lifetimes," in *Proceedings of the Eighth International Conference on Information and Management Sciences*, pp. 794–797, Kunming, China, September 2009.

[26] B. Xiao-ping, Z. Yu-hong, and L. Ya-nan, "A novel approach to study real-time dynamic optimization analysis and simulation of complex mine logistics transportation hybrid system with belt and surge links," *Discrete Dynamics in Nature and Society*, vol. 2015, Article ID 601578, 8 pages, 2015.

[27] L. Y. Zhang, T. Fei, and Y. S. Sun, "The Research about simulated annealing ant colony algorithm in emergency logistics path optimization," *Advanced Materials Research*, vol. 482–484, pp. 2470–2474, 2012.

[28] Z. C. Hua, H. Xin, and Z. Wei, "Logistics distribution routing optimization algorithm," *Applied Mechanics and Materials*, vol. 513–517, pp. 1740–1743, 2014.

Hindawi
Mathematical Problems in Engineering
Volume 2019, Article ID 2892545, 9 pages
https://doi.org/10.1155/2019/2892545

Research Article

Spatial Reasoning Based on 3D-ICSRM Model

Yongshan Liu,[1] Xiang Gong,[1] and Dehan Kong[2]

[1]*Department of Information Science and Engineering, Yanshan University, Hebei Street No. 438, Qinhuangdao, Hebei 066004, China*
[2]*Department of Information Engineering, Hebei University of Environmental Engineering, Jingang Street No. 8, Qinhuangdao, Hebei 066102, China*

Correspondence should be addressed to Xiang Gong; alan0432@qq.com

Received 27 March 2019; Revised 9 May 2019; Accepted 24 June 2019; Published 18 July 2019

Guest Editor: Federico Divina

The existing spatial relationship composite models have defects in both cognitive habits and differentiation degree when describing the spatial relationship between the three dimensional objects. These defects can cause inaccuracy in the process of spatial reasoning. In order to solve this problem, this paper proposes a Three-Dimensional Improved Composite Spatial Relationship Model (3D-ICSRM). Then a high-precision spatial relationship reasoning algorithm is presented based on this model, which combines qualitative and quantitative analyses. Finally, both the correctness and performance advantages of spatial reasoning algorithm are verified by experiments based on this proposed model.

1. Introduction

The representation and reasoning of spatial information is the core of Artificial Intelligence system, Geographic Information System (GIS), and so on [1]. In order to make better use of the spatial information in practice, it is of importance to understand, describe, analyze, and process the spatial relationship accurately [2]. Spatial relationship expression model is the basis of describing and analyzing the spatial relationship between objects in GIS. Single-mode spatial relationship model is lack of the accuracy of describing the relationship between objects and completeness of expressing the spatial information. Therefore, the research of spatial relationship tends to compound model in recent years. At present, there are three limitations in the study of the compound expression model: (1) Cognitive view: although the size of the object itself is considered, there is a big difference between the definition of the direction and the human cognitive habit which leads to serious semantic conflict in the process of spatial relation reasoning [3]. (2) Differentiation degree: the spatial location information is described with low accuracy which can lead to large errors in the calculation processing and obvious limitations in solving complex spatial relationships. (3) Spatial dimension: there are few studies on three-dimensional space due to the fact that the present research mainly focuses on the two-dimensional space. In summary, in small scale three-dimensional space, spatial object is often represented as a point, rather than the influence of the shape and size of the object itself [4]. Therefore, the spatial relation model in this environment has higher requirements in terms of spatial cognition and division. This paper proposes a compound 3D spatial relation model named Three-Dimensional Improved Composite Spatial expression Relationship Model (3D-ICSRM) to solve the problem. Moreover, a new high-precision algorithm of position relation reasoning is presented on the basis of this model. The remainder of the paper is organized as follows: Section 2 reviews related works of spatial relationship. Section 3 proposes the 3D-ICSRM model and evaluates the performance of the model. Section 4 presents a high-precision spatial relation reasoning algorithm based on the description of spatial information. Section 5 provides the reasoning results, verifies the correctness of the composite model and reasoning algorithm, and presents the advantages of the inference algorithm over composite table method by using comparison experiments. Section 6 summarizes the work of this paper and presents an outlook for future works.

2. Related Works

At present, the common composite methods of 3D spatial relations are projection-matrix method, direction-topological method, and direction-distance method. In the

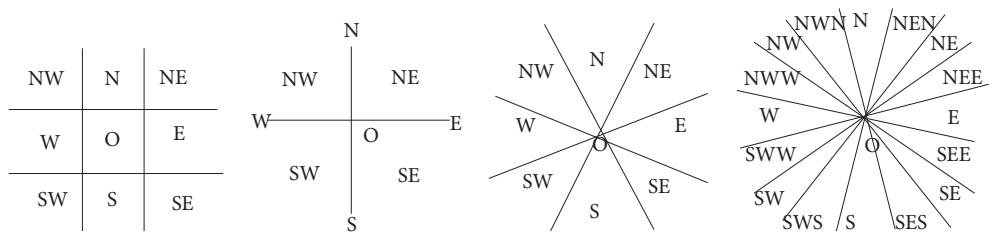

(a) MBR model (b) 8-direction cone model A (c) 8-direction cone model B (d) 16-direction cone model

Figure 1: Models of spatial direction relations.

aspect of projection-matrix method, Chen et al. [5] used the intersection cube matrix to describe the directional relationship in 3D space. Wang et al. [6] represented 3D spatial directional relationship with a 3x9 matrix and gave the corresponding reasoning method. Gu et al. [7] applied the double-projection 3x3 matrix model to describe the directional relationship. Spatial objects were represented by the Minimum Bounding Rect (MBR) in all of the above models as shown in Figure 1(a). Obviously, there is a difference between the definition of direction in these MBR-based models and human cognitive habits. People do not describe North in such a rigid way as MBR-based model does. There are a lot of researches on the combination of direction and topology. Song et al. [8] proposed an effective complex spatial relationship model named TDSC based on the relationship of topology, direction, and size. Li et al. [9] presented a consistency algorithm to deal with the constraints of topological relationship and directional relationship. Salamat et al. [10] proposed a method for reasoning of two dimensional spatial scenes with the Combination of Topological Direction (CTD) to handle the combination of topological and directional relationships. However, these models are still imprecise when describing the qualitative relationship between spatial objects. In the study of the composite model of directional relationship and distance relationship, Liu et al. [11] proposed a combination of directional model and qualitative distance as shown in Figure 1(b). Although this model has some improvement in cognition, it still has some shortcomings as inaccuracy for the division and description of the direction. Li et al. [12] presented 3DR44-4d model by adding distance relationship into 3DR44 model. This model increased the accuracy of the expression. Meanwhile, the division and cognition of spatial directional relationship have not been improved effectively. Wang et al. [13] combined the 8-direction cone model with the distance relationship as shown in Figure 1(c). However, the model can only be applied to 2D spatial objects, and the position information of 3D spatial objects cannot be expressed correctly in these models. These defects affect the accuracy of spatial reasoning results directly. More and more attention has been paid to the processing of complex spatial information [14]. As a result, there is a higher requirement for the three-dimensional spatial relationship model in the aspect of both cognition and accuracy. However, the existing models are deficient. To solve this problem, this paper proposes a three-dimensional improved composite spatial relationship model (3D-ICSRM) and presents a new algorithm for high-precision spatial relation reasoning.

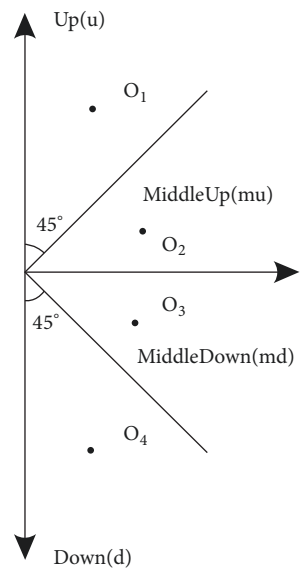

Figure 2: 4 layers.

3. 3D-ICSRM Model

The cone model is more suitable for human cognition than other models in the definition of the spatial directional relationship, and it is easy to implement and maintain. The comparison of the three cone models showed in Figures 1(b), 1(c), and 1(d) shows that the cone model in Figure 1(c) is better than other models in space division. Therefore, this paper presents 3D-ICSRM based on the model shown in Figure 1(c). The 3D-ICSRM model is shown in Figure 5.

Definition 1. 4 Layers. Define 4 layers as Up (Abbreviations: *u*), MiddleUp (Abbreviations: *mu*), MiddleDown (Abbreviations: *md*), and Down (Abbreviations: *d*), which fits our cognition in verticle.

As Is Shown in Figure 2. The space in verticle is divided into 4 layers, which are *u*, *mu*, *md*, and *d*. Layer *u* and layer *mu* are divided by a line which is angled 45 degrees from the x-axis. As the same reason layer *md* and layer *d* are divided.

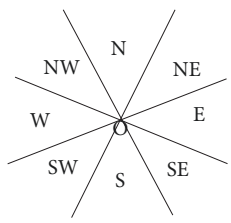

Figure 3: 8 directional areas.

There are four objects O_1, O_2, O_3, and O_4 in this area, and they are in u, mu, md, and d separately.

Definition 2. 8 Directional Areas. Define 8 directional areas as North (Abbreviations: N), NorthWest (Abbreviations: NW), West (Abbreviations: W), SouthWest (Abbreviations: SW), South (Abbreviations: S), SouthEast (Abbreviations: SE), East (Abbreviations: E), and NorthEast (Abbreviations: NE), which fits our cognition in horizontal.

As Is Shown in Figure 3. The spaces in one level are separated into N, NW, W, SW, S, SE, E, and NE 8 directional areas.

Definition 3. 5 Qualitative Distances. Define 5 qualitative distance areas as veryclose (q_0=[0, k_1)), close (q_1=[k_1, k_2)), intermediate (q_2=[k_2, k_3)), far (q_3=[k_3, k_4)), and veryfar (q_4=[k_4, ∞)) (k_1,k_2,k_3,k_4 ϵ (0,∞)), which close to our real life.

For example, when the distance between me and the storm is 0m to 100m, I would say it is very close to me. While when the distance changes to 100m to 500m, I claim it is close to me. More than, 500m to 1000m is intermediate for me. 1000m to 1500m is far for me. As for the distance up to 1500m, it is very far for me. Take this as an example; when I set my qualitative distance, I would set q_0=[0,100), q_1=[100,500),q_2=[500,1000),q_3=[1000,1500), and q_4=[1500,∞). 5 qualitative distances change with the domain of the observer's cognition for distance in real. As Is Shown in Figure 4. The distance of one direction is divided into 5 areas, which means veryclose (q_0), close (q_1), intermediate (q_2), far (q_3), and veryfar (q_4).

Definition 4. 3D-ICSRM Model. Based on the above three definitions, in three-dimensional space, with the reference object as the center, three-dimensional space is divided into $4 * 8 * 5$ areas (4 layers combine 8 directional areas and combine 5 qualitative distances). Point O(x,y,z) represents the centroid of a three-dimensional object. And 4 layers combine 8 directional areas; divide the three-dimensional space into 32 areas as follows:

$$
\begin{cases} Nu, & (x,y)\,\epsilon\left(\frac{3\pi}{8},\frac{5\pi}{8}\right], z\epsilon\left(0,\frac{\pi}{4}\right] \\ Nmu, & (x,y)\,\epsilon\left(\frac{3\pi}{8},\frac{5\pi}{8}\right], z\epsilon\left(\frac{\pi}{4},\frac{\pi}{2}\right] \\ Nmd, & (x,y)\,\epsilon\left(\frac{3\pi}{8},\frac{5\pi}{8}\right], z\epsilon\left(\frac{\pi}{2},\frac{3\pi}{4}\right] \\ Nd, & (x,y)\,\epsilon\left(\frac{3\pi}{8},\frac{5\pi}{8}\right], z\epsilon\left(\frac{3\pi}{4},\pi\right], \end{cases}
\begin{cases} NWu, & (x,y)\,\epsilon\left(\frac{5\pi}{8},\frac{7\pi}{8}\right], z\epsilon\left(0,\frac{\pi}{4}\right] \\ NWmu, & (x,y)\,\epsilon\left(\frac{5\pi}{8},\frac{7\pi}{8}\right], z\epsilon\left(\frac{\pi}{4},\frac{\pi}{2}\right] \\ NWmd, & (x,y)\,\epsilon\left(\frac{5\pi}{8},\frac{7\pi}{8}\right], z\epsilon\left(\frac{\pi}{2},\frac{3\pi}{4}\right] \\ NWd, & (x,y)\,\epsilon\left(\frac{5\pi}{8},\frac{7\pi}{8}\right], z\epsilon\left(\frac{3\pi}{4},\pi\right], \end{cases}
$$

$$
\begin{cases} Wu, & (x,y)\,\epsilon\left(\frac{7\pi}{8},\frac{9\pi}{8}\right], z\epsilon\left(0,\frac{\pi}{4}\right] \\ Wmu, & (x,y)\,\epsilon\left(\frac{7\pi}{8},\frac{9\pi}{8}\right], z\epsilon\left(\frac{\pi}{4},\frac{\pi}{2}\right] \\ Wmd, & (x,y)\,\epsilon\left(\frac{7\pi}{8},\frac{9\pi}{8}\right], z\epsilon\left(\frac{\pi}{2},\frac{3\pi}{4}\right] \\ Wd, & (x,y)\,\epsilon\left(\frac{7\pi}{8},\frac{9\pi}{8}\right], z\epsilon\left(\frac{3\pi}{4},\pi\right], \end{cases}
\begin{cases} SWu, & (x,y)\,\epsilon\left(\frac{9\pi}{8},\frac{11\pi}{8}\right], z\epsilon\left(0,\frac{\pi}{4}\right] \\ SWmu, & (x,y)\,\epsilon\left(\frac{9\pi}{8},\frac{11\pi}{8}\right], z\epsilon\left(\frac{\pi}{4},\frac{\pi}{2}\right] \\ SWmd, & (x,y)\,\epsilon\left(\frac{9\pi}{8},\frac{11\pi}{8}\right], z\epsilon\left(\frac{\pi}{2},\frac{3\pi}{4}\right] \\ SWd, & (x,y)\,\epsilon\left(\frac{9\pi}{8},\frac{11\pi}{8}\right], z\epsilon\left(\frac{3\pi}{4},\pi\right], \end{cases} \tag{1}
$$

$$
\begin{cases} Su, & (x,y)\,\epsilon\left(\frac{11\pi}{8},\frac{13\pi}{8}\right], z\epsilon\left(0,\frac{\pi}{4}\right] \\ Smu, & (x,y)\,\epsilon\left(\frac{11\pi}{8},\frac{13\pi}{8}\right], z\epsilon\left(\frac{\pi}{4},\frac{\pi}{2}\right] \\ Smd, & (x,y)\,\epsilon\left(\frac{11\pi}{8},\frac{13\pi}{8}\right], z\epsilon\left(\frac{\pi}{2},\frac{3\pi}{4}\right] \\ Sd, & (x,y)\,\epsilon\left(\frac{11\pi}{8},\frac{13\pi}{8}\right], z\epsilon\left(\frac{3\pi}{4},\pi\right], \end{cases}
\begin{cases} SEu, & (x,y)\,\epsilon\left(\frac{11\pi}{8},\frac{13\pi}{8}\right], z\epsilon\left(0,\frac{\pi}{4}\right] \\ SEmu, & (x,y)\,\epsilon\left(\frac{11\pi}{8},\frac{13\pi}{8}\right], z\epsilon\left(\frac{\pi}{4},\frac{\pi}{2}\right] \\ SEmd, & (x,y)\,\epsilon\left(\frac{11\pi}{8},\frac{13\pi}{8}\right], z\epsilon\left(\frac{\pi}{2},\frac{3\pi}{4}\right] \\ SEd, & (x,y)\,\epsilon\left(\frac{11\pi}{8},\frac{13\pi}{8}\right], z\epsilon\left(\frac{3\pi}{4},\pi\right], \end{cases}
$$

$$
\begin{cases} NEu, & (x,y)\,\epsilon\left(\frac{\pi}{8},\frac{3\pi}{8}\right], z\epsilon\left(0,\frac{\pi}{4}\right] \\ NEmu, & (x,y)\,\epsilon\left(\frac{\pi}{8},\frac{3\pi}{8}\right], z\epsilon\left(\frac{\pi}{4},\frac{\pi}{2}\right] \\ NEmd, & (x,y)\,\epsilon\left(\frac{\pi}{8},\frac{3\pi}{8}\right], z\epsilon\left(\frac{\pi}{2},\frac{3\pi}{4}\right] \\ NEd, & (x,y)\,\epsilon\left(\frac{\pi}{8},\frac{3\pi}{8}\right], z\epsilon\left(\frac{3\pi}{4},\pi\right], \end{cases}
\begin{cases} Eu, & (x,y)\,\epsilon\left(\frac{15\pi}{8},2\pi\right], z\epsilon\left(0,\frac{\pi}{4}\right] \\ Emu, & (x,y)\,\epsilon\left(\frac{15\pi}{8},2\pi\right], z\epsilon\left(\frac{\pi}{4},\frac{\pi}{2}\right] \\ Emd, & (x,y)\,\epsilon\left(\frac{15\pi}{8},2\pi\right], z\epsilon\left(\frac{\pi}{2},\frac{3\pi}{4}\right] \\ Ed, & (x,y)\,\epsilon\left(\frac{15\pi}{8},2\pi\right], z\epsilon\left(\frac{3\pi}{4},\pi\right]. \end{cases}
$$

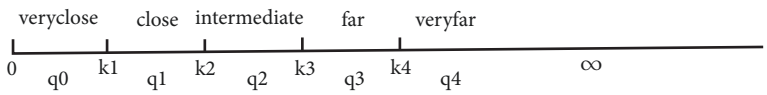

Figure 4: 5 qualitative distances.

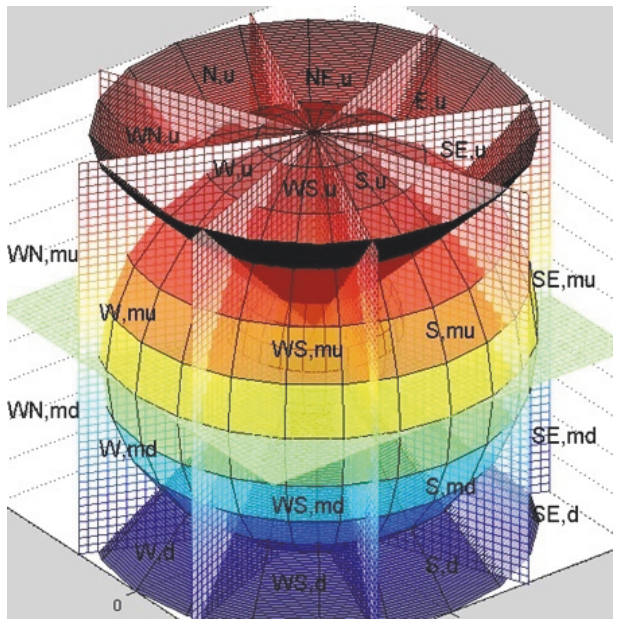

Figure 5: Improved Composite Spatial Relationship Model of 3D.

The 3D-ICRSM model includes 4 layers in vertical. Each level of horizontal is divided into 8 directional areas average. Each part of the 32 separated areas in the three-dimensional space has 5 qualitative distances. Thus through this model, each object's direction can be described easily. The schematic diagram of the 3D-ICSRM is shown in Figure 5.

The distance between the adjacent qualitative areas meets a fixed proportion of k ($k \epsilon N^+$). D_3 is used to represent the 32 directional regions around the reference object while d_3 is the symbol set of the 5 distance regions. Take the map as an example; the scale is smaller and the content is more detailed. On the contrary, the scope is larger and the content is simple. The 5 evaluation indexes of the model proposed by Goyal are an important basis for evaluating the performance of a spatial relation model [15]. The following is a theoretical analysis of the performance of the model from five aspects: (1) Formal. The directional terminology used by people to communicate with each other may have different meanings for different people, but in GIS it is necessary to have a formal definition of the direction terms, which can be used to formalize the model. The definitions of 3D-ICSRM in both horizontal and vertical direction are more in line with the spatial cognition of human daily habits. Combined with the rigorous qualitative distance of the space division, the formal ability is well. (2) Inferential. The spatial relation model has the ability to infer the unknown spatial relationship from the spatial relations among the known spatial objects and obtain the relationship between other objects. There is an accurate range and range of distances for each spatial region of the 3D-ICSRM model. If there is no coincidence, there will be 25600 kinds of reasoning results. (3) Shape-Sensitive. The result is the same when the model describes objects at different observation scales. Because of the limitation of the cone model in describing spatial relations, the 3D-ICSRM model can only be used to describe and define the spatial relations between three dimensional objects in a small scale environment. (4) Dimension-Neutral. The space object is treated as a point in the cone model, and the shape of the object does not have a great influence on the judgment of the spatial relationship. Therefore, the 3D-ICSRM model does not consider the shape of the reference object. (5) Comparable. Due to the increase of the horizontal and vertical division of the 3D-ICSRM model, there are 160 kinds of position relations that can be distinguished directly.

4. Reasoning

4.1. Principle of Reasoning Method. Reasoning is deriving unknown directions from the known directions. As shown in Formula (2). The spatial relationship between object A and object C could be inferred by two known directions $q_i dir(A, B)$ and $q_j dir(B, C)$. Here $dir(A, B)$ means the direction of two objects in three-dimensional, $directions(A, B)$

abbreviations: $dir(A, B)$. The symbol $\wedge$ means combine two directions of reasoning. $\longrightarrow$ is a deduced symbol which means one can derive results from combined conditions. d_{AC} means the distance between objects A and C; it represents the abbreviation of $distance_{AC}$.

$$q_i dir\,(A, B) \wedge q_j dir\,(B, C) \longrightarrow d_{AC} dir\,(A, C) \tag{2}$$

In the 3D-ICSRM model and the spherical coordinate system, angle α,β and distance d are used to describe the relationship between the Target Object (TO) and the Reference Object (RO). Angle α represents 8 horizontal regions: N represents $(3\pi/8, 5\pi/8]$, NW represents $(5\pi/8, 7\pi/8]$, W represents $(7\pi/8, 9\pi/8]$, SW represents $(9\pi/8, 11\pi/8]$, S represents $(11\pi/8, 13\pi/8]$, SE represents $(13\pi/8, 15\pi/8]$, NE represents $(\pi/8, 3\pi/8]$, and E represents $(15\pi/8, 2\pi]$. Angle β represents 4 vertical regions: u represents $(0, \pi/4])$, mu represents $(\pi/4, \pi/2])$, md represents $(\pi/2, 3\pi/4])$, and d represents $(3\pi/4, \pi])$. d represents qualitative distance between the TO and RO. Thus $\alpha\epsilon\{N,S,E,W,NE,NW,SE,SW\}$, $\beta\epsilon\{u, mu, md, d\}$, and $d\epsilon d_3$. The conversion formula between spherical coordinates and Cartesian coordinates is shown as Formula (3). α, β indicate the angle between the object and the three-dimensional Cartesian axis.

$$\begin{aligned} x &= r \sin\beta \cos\alpha \\ y &= r \sin\beta \sin\alpha, \quad r \geq 0,\ \beta\ \epsilon\,(0, \pi]\,, \alpha\ \epsilon\,(0, 2\pi] \\ z &= r \cos\beta \end{aligned} \tag{3}$$

The coordinate of object A is (x_A, y_A,z_A), and the coordinate of object B is (x_B, y_B, z_B); then the spherical coordinates are shown in Formula (4). d_{AB} means the distance of object A and object B in three-dimensional space.

$$\begin{aligned} x_B - x_A &= d_{AB} \sin\beta_A \cos\alpha_A \\ y_B - y_A &= d_{AB} \sin\beta_A \sin\alpha_A, \\ &\qquad d_{AB}\epsilon d,\ \beta_A\epsilon\,(0, \pi]\,,\ \alpha_A\epsilon\,(0, 2\pi] \\ z_B - z_A &= d_{AB} \cos\beta_A \end{aligned} \tag{4}$$

Set object C as (x_C, y_C,z_C); then the relationship between C and B meets Formula (5).

$$\begin{aligned} x_C - x_B &= d_{BC} \sin\beta_B \cos\alpha_B \\ y_C - y_B &= d_{BC} \sin\beta_B \sin\alpha_B, \\ &\qquad d_{BC}\epsilon d,\ \beta_B\epsilon\,(0, \pi]\,,\ \alpha_B\epsilon\,(0, 2\pi] \\ z_C - z_B &= d_{BC} \cos\beta_B \end{aligned} \tag{5}$$

Meanwhile, the relationship between C and A meets Formula (6).

$$\begin{aligned} x_C - x_A &= (x_C - x_B) + (x_B - x_A) \\ y_C - y_A &= (y_C - y_B) + (y_B - y_A) \\ z_C - z_A &= (z_C - z_B) + (z_B - z_A) \end{aligned} \tag{6}$$

So the reasoning is shown in Formula (7).

$$\begin{aligned} x_C - x_A &= d_{AB} \sin\beta_A \cos\alpha_A + d_{BC} \sin\beta_B \cos\alpha_B \\ y_C - y_A &= d_{AB} \sin\beta_A \sin\alpha_A + d_{BC} \sin\beta_B \sin\alpha_B, \\ &\qquad d_{AB}, d_{BC}\epsilon d,\ \beta_A, \beta_B\epsilon\,(0, \pi]\,,\ \alpha_A, \alpha_B\epsilon\,(0, 2\pi] \\ z_C - z_A &= d_{AB} \cos\beta_A + d_{BC} \cos\beta_B \end{aligned} \tag{7}$$

The angle α_A is included angle between segment AB and line $\{y = y_A, z = z_A\}$ positive while the angle α_B is included angle between segment BC and line $\{x = x_B, z = z_B\}$ positive. The angle β_A is included angle between AB and line $\{x = x_A, y = y_A\}$ positive while the angle β_B is included angle between BC and line $\{x = x_B, y = y_B\}$ positive. For example, when the coordinate of object A is origin, then the line $\{y = y_A, z = z_A\}$. Based on the 3D-ICSRM model, the qualitative distance satisfies the following three limitations: (1) Monotone increasing. $q(k_1) \leq q(k_2), \forall k_1, k_2\epsilon N^+, k_1 \leq k_2$. (2) The range of a given distance is greater than that of all previous ranges which can be expressed as $q_i \geq \Delta i - 1, i \geq 1$. (3) The absorption rate. Define ">>" as a logical relation, $\forall\varepsilon > 0$; if $q_i/q_j \geq \varepsilon$, then $q_i >> q_j$. If $q_i >> q_j$, then $q_i \pm q_j \approx q_i$. q_j is "absorbed."

4.2. The Algorithm of HPSRA. Consider the definition and description of spatial 3D-ICSRM model and spatial relation reasoning principle proposed in the previous section. The reasoning algorithm of HPSRA (High-precision Spatial Reasoning Algorithm) based on 3D-ICSRM is presented (See Algorithm 1). The main ideas of the algorithm are as follows: Step1: The establishment of a spatial relationship model. The 3D-ICSRM model is constructed based on the reference object. The space around reference object is divided into 4 levels, each level contains 8 directions, and each direction contains 5 sections of qualitative distance range, as a total of 160 kinds of space area. Step2: Spatial relation reasoning. Based on the 3D-ICSRM model, judge whether there is the phenomenon of "absorption" in the distance relation of known spatial objects. If there is absorption, the position relation of an unknown object is equal to the position relation of the object with a large distance. Otherwise, the reasoning of the location relation of unknown objects in space is deduced based on the reasoning principle proposed in preceding 4.1. Step3: Processing of result sets. According to the definition of the model in Step1, we can judge the locations of all the elements in Step2 and then infer all possible spatial position relationships of the unknown objects according to the region type.

In 1st line, the definition of the 3D-ICSRM model is given. Then the spatial position relation between objects A and B, B and C is given based on the model. From 6th to 9th lines of code is used to judge whether the known position satisfies the constraint conditions of qualitative distance. The numerical calculation of the relative relation of the implicit object is done from 11th line to 13th line. The calculations of all results angles and distances are done from 13th line to 15th line. Then, the distance relationship is got in 18th line, and directional

Input: The location relationship between A and B:the distance of A and B (abbreviations: $dis_{A,B}$),the direction of A and B(abbreviations: $dir_{A,B}$);
The location relationship between B and C: $dis_{B,C}$, $dir_{B,C}$
Output: The location relationship between A and C: $dis_{A,C}$, $dir_{A,C}$
1: Create Model
2: $a_i, a_{i+1} \longleftarrow$ Init$dis_{A,B}$(Init means initialize the distance between two objects)
3: $a_j, a_{j+1} \longleftarrow$ Init$dis_{B,C}$
4: $\alpha_A, \beta_A \longleftarrow dir_{A,B}$
5: $\alpha_B, \beta_B \longleftarrow dir_{B,C}$
6: IF $(a_{i+1}/a_{j+1} \geq k^2)$
7: $dis_{A,C}= dis_{A,B}$ and $dir_{A,C}= dir_{A,B}$
8: ELSE IF$(a_{j+1}/a_{i+1} \geq k^2)$
9: $dis_{A,C}= dis_{B,C}$ and $dir_{A,C}= dir_{B,C}$
10: ELSE
11: $x_C, y_C, z_C \longleftarrow Reason(a_i, a_{i+1}, a_j, a_{j+1}, \alpha_A, \beta_A, \alpha_B, \beta_B)$(*Reason* means conduct spatial direction relationship reasoning)
12: $list.add()$
13: **for** $i = 0; i < list.Count - 1; i++$ **do**
14: $a_n, a_{n+1}, \alpha_C, \beta_C \longleftarrow Reason(List(i))$
15: $list.add()$
16: **end for**
17: **for** $j = 0; j < list.Count - 1; j++$ **do**
18: $dis_{A,C} \longleftarrow Caldis(list(j))$(*Caldis* means Calculate the distance)
19: $dir_{A,C} \longleftarrow Caldir(list(j))$(*Caldir* means Calculate the dirtional relationship)
20: **end for**
21: Return $dis_{A,C}$, $dir_{A,C}$

Algorithm 1: The algorithm Of HPSRA.

Table 1: Reasoning result of q_iNu, q_jEmd.

	q_0Emd	q_1Emd	q_2Emd	q_3Emd	q_4Emd
q_0Nu	$q_0\|q_1$ *NUEMD*	$q_0\|q_1\|q_2$ *NUEMD_EMD*	q_2Emd	q_3Emd	q_4Emd
q_1Nu	$q_0\|q_1\|q_2$ *NUEMD_NU*	$q_0\|q_1\|q_2$ *NUEMD*	$q_1\|q_2\|q_3$ *NUEMD_NU*	q_3Emd	q_3Emd
q_2Nu	q_2Nu	$q_1\|q_2\|q_3$ *NUEMD_NU*	$q_1\|q_2\|q_3$ *NUEMD*	$q_2\|q_3\|q_4$ *NUEMD_NU*	q_4Emd
q_3Nu	q_3Nu	q_3Nu	$q_2\|q_3\|q_4$ *NUEMD_NU*	$q_2\|q_3\|q_4$ *NUEMD*	$q_3\|q_4$ *NUEMD_EMD*
q_4Nu	q_4Nu	q_4Nu	q_4N	$q_3\|q_4$ *NUEMD_NU*	$q_3\|q_4$ *NUEMD*

relationship is calculated in 19th line. Finally, the location relationship of objects A and C is returned in 21st line.

The advantages of reasoning algorithm for 3D location relation based on spatial compound expression model are obvious. The model 3D-ICSRM is used to describe the spatial relationships between A, B, and C, which are consistent with human cognition and have a high degree of similarity to similar spatial relationships, providing a detailed description of the spatial relationship information and reasoning for the calculation of the premise. Consider the restriction mechanism of spatial relation, calculation principle, and conversion formula, and use quantitative calculation of qualitative distance constraints and 3D object position by way of objects A, C spatial relation reasoning. The reasoning process is a precise numerical calculation. Therefore, the inference results are more accurate with less error. The quantitative calculation results are returned and the spatial region is judged and described based on the 3D-ICSRM model. Finally, the spatial position relationship between A and C is obtained.

5. Experimental Results and Analysis

5.1. Reasoning Method Verification. The development environment of prototype reasoning system based on compound model is Microsoft Visual Studio 2010 and Matlab R2012a. When $dir_{(C,B)} = q_iNu$, $dir_{(B,A)} = q_jEmd$, then $dir_{(C,A)}= dir_{(C,B)}dir_{(B,A)}=q_iNuq_jEmd$. The result of reasoning is shown in Table 1. Note: *NUEMD*={*Eu*, *Emd*, *NEu*, *NEmu*, *Emu*, *NEmd*, *Nu*, *Nmu*}. *NUEMD_NU*={*Eu*,

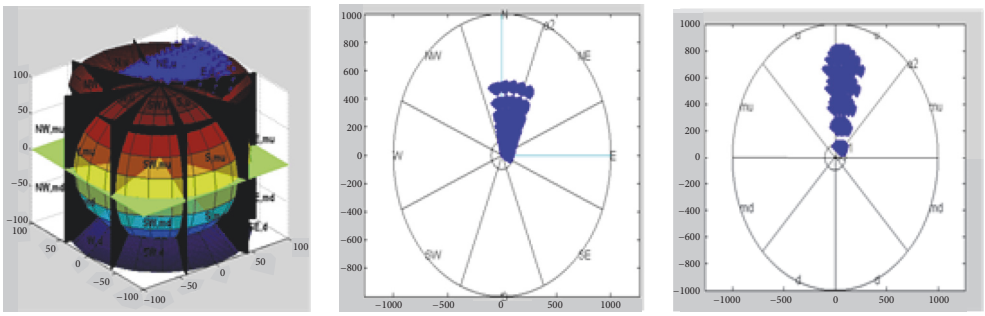

(a) Reasoning in 3D space (b) Reasoning in XOY plane (c) Reasoning in XOZ plane

Figure 6: The result of point cloud rabbit registration.

Table 2: The comparison of different reasoning result ($i = j$).

Methods	$i = 0, j = 0$	$i = 1, j = 1$	$i = 2, j = 2$	$i = 3, j = 3$	$i = 4, j = 4$
HPSRA	$q_0\|q_1$	$q_0\|q_1\|q_2$	$q_1\|q_2\|q_3$	$q_2\|q_3\|q_4$	$q_3\|q_4$
	NUEMD	*NUEMD*	*NUEMD*	*NUEMD*	*NUEMD*
ComplexTables	$q_0\|q_1$	$q_0\|q_1\|q_2$	$q_0\|q_1\|q_2\|q_3$	$q_0\|q_1\|q_2\|q_3\|q_4$	$q_0\|q_1\|q_2\|q_3\|q_4$
	*NUEMD*1	*NUEMD*1	*NUEMD*1	*NUEMD*1	*NUEMD*1

Table 3: The comparison of different reasoning result ($i = j + 1$).

Methods	$i = 1, j = 0$	$i = 2, j = 1$	$i = 3, j = 2$	$i = 4, j = 3$
HPSRA	$q_0\|q_1\|q_2$	$q_1\|q_2\|q_3$	$q_2\|q_3\|q_4$	$q_3\|q_4$
	NUEMD_NU	*NUEMD_NU*	*NUEMD_NU*	*NUEMD_NU*
ComplexTables	$q_0\|q_1\|q_2$	$q_0\|q_1\|q_2\|q_3$	$q_0\|q_1\|q_2\|q_3\|q_4$	$q_0\|q_1\|q_2\|q_3\|q_4$
	*NUEMD*1	*NUEMD*1	*NUEMD*1	*NUEMD*1

Table 4: The comparison of different reasoning result ($j = i + 1$).

Methods	$i = 0, j = 1$	$i = 1, j = 2$	$i = 2, j = 3$	$i = 3, j = 4$
HPSRA	$q_0\|q_1\|q_2$	$q_1\|q_2\|q_3$	$q_2\|q_3\|q_4$	$q_3\|q_4$
	NUEMD_EMD	*NUEMD_EMD*	*NUEMD_EMD*	*NUEMD_EMD*
ComplexTables	$q_0\|q_1\|q_2$	$q_0\|q_1\|q_2\|q_3$	$q_0\|q_1\|q_2\|q_3\|q_4$	$q_0\|q_1\|q_2\|q_3\|q_4$
	*NUEMD*1	*NUEMD*1	*NUEMD*1	*NUEMD*1

Emu, *NEu*, *NEmu*, *Nu*, *Nmu*}. *NUEMD_EMD*={*Eu*, *Emu*, *Emd*,*NEmu*, *NEmd*}.

According to Table 1, we can draw the following rules of reasoning results: (1) if $i = j$, then $q_i Nu \wedge q_j Emd \longrightarrow q_{i-1}/q_i/q_{i+1}Eu$, *Emu*, *Emd*, *NEu*, *NEmu*, *NEmd*,*Nu*, *Nmu*. (2) If $i = j + 1$, then $q_i Nu \wedge q_j Emd \longrightarrow q_{i-1}/q_i/q_{i+1}Eu$, *Emu*, *NEu*, *NEmu*, *Nu*, *Nmu*. The reasoning result of *Nu* and *Emd* is biased in the direction of *Nu*. (3) If $j = i + 1$, then $q_i N \wedge q_j Emd \longrightarrow q_{j-1}/q_j/q_{j+1}Eu$, *Emu*, *Emd*, *NEmu*, *NEmd*. The reasoning result of *Nu* and *Emd* is biased in the direction of *Emd*. (4) $|i - j| = 2$, $q_i N \wedge q_j Emd \longrightarrow q_i Nu$ or $q_i N$,$q_j Emd \longrightarrow q_j Emd$. The image simulations of $q_2 Nu$ and $q_1 Emd$ reasoning results in different dimensions are shown in Figure 6. Based on the 3D-ICSRM model, there are 160∗160 kinds of combination types in 3D spatial reasoning, which is consistent with the above inference principle. This section does not list one by one.

5.2. Comparison and Analysis of Reasoning Methods. In order to analyze the performance of HPSRA clearly, the comparative experiment is given between algorithm HPSRA and the complex tables method based on the 3D-ICSRM. Complex Tables Method (CTM) is a frequently-used method for spatial relation reasoning. The reasoning of positional relation under the CTM is a combination of distance relation and direction relation, which can get the results of valid inference. Tables 2, 3, and 4 give the comparisons of the two methods under the conditions $i = j$, $i = j + 1$, $i = j - 1$ when reasoning $q_i Nu$ and $q_j Emd$.

Note:*NUEMD*1={*Nu*, *Nmu*, *Nmd*, *NEu*, *NEmu*, *NEmd*, *Eu*, *Emu*, *Emd*}. Comparing the results under the conditions $i = j$, $i = j + 1$, and $i = j - 1$ in Table 2, we can conclude that the HPSRA algorithm has the following advantages compared with the CTM:

(1) Higher Accuracy. There are different results in the result of HPSRA algorithm based on the distance between objects. For example, when the distance is equal that i=j, reasoning results for all possible directions, when the distance range is $|i - j| = 1$, the result of direction relations tends to the side distance range of Nu or Emd. Both the horizontal and vertical directions are satisfied. The fundamental reason is that the HPSRA algorithm takes into account the two constraints in the reasoning process: the distance and the direction. CTM is only a combination of two spatial relations, without considering the interaction between the two spatial relations. Therefore, the HPSRA algorithm is more accurate.

Note: $NUEMD1$={Nu, Nmu,Nmd,NEu, $NEmu$,$NEmd$, Eu,Emu, Emd}

Note: $NUEMD1$={Nu, Nmu, Nmd, NEu, $NEmu$, $NEmd$, Eu, Emu, Emd}

(2) The scope is smaller, and the error is less. From Tables 2, 3, and 4 comparison results can be seen: under the conditions $i = j$, $i = j + 1$, and $i = j - 1$. The result of HPSRA algorithm about the location of unknown space objects is smaller than the composite tables method. Because of the definition of spatial relations, 3D-ICSRM uses a semiclosed definition such as $q_2 \epsilon (k, k^2]$, $\alpha_A \epsilon (3\pi/8, 5\pi/8]$,$\beta_A \epsilon (0, \pi/4]$. The HPSRA algorithm is used to solve the boundary problem. The boundary generated by the inference process has a clear definition of which spatial relations belong to it. So the result of HPSRA algorithm is smaller with less error.

(3)Stronger Regularity. The HPSRA algorithm, when $i = j$, results for $q_{i-1}/q_i/q_{i+1}NUEMD$. When $i = j + 1$, the result of reasoning is $q_{i-1}/q_i/q_{i+1}NUEMD\_NU$, and the direction of the direction is biased to the side of Nu. When $j = i + 1$, inference results for $q_{j-1}/q_j/q_{j+1}NUEMD\_NU$, and there is a strong regularity in the direction of the deviation of the direction of Emd. CTM results for all the directions. When the distance is greater than q_3, it is close to the complete set.

6. Conclusion

In this paper, aiming at the shortcomings of the existing 3D spatial compound expression model in the accurate description of position information and the practical application, a new model 3D-ICSRM of three-dimensional spatial relations is proposed, which is consistent with human cognitive habits and spatial division. Based on the compound expression model, the method of qualitative description and quantitative reasoning of HPSRA is given. This paper presents a kind of high precision spatial reasoning algorithm based on the mutual restriction mechanism of different spatial relations, the principle of 3D coordinate transformation, and the formula of calculation. Finally, based on 3D-ICSRM, the results of HPSRA algorithm and CTM are compared. The results show that the method proposed in this paper has obvious advantages in terms of accuracy, range, error, and regularity. The research work in the future will focus on the use of composite model 3D-ICSRM combined with spatial index technology for three-dimensional spatial data query.

Data Availability

No data were used to support this study.

Conflicts of Interest

The authors declare that there are no conflicts of interest regarding the publication of this paper.

Acknowledgments

This work is supported by the Natural Science Foundation of Hebei Province, China, under Grant No. F2017203019.

References

[1] A. G. Cohn and J. Renz, "Qualitative spatial representation and reasoning," in *Handbook of Knowledge Representation*, F. V. Harmelen et al., Ed., vol. 3 of *Foundations of Artificial Intelligence*, pp. 551–596, Elsevier, 2008.

[2] C. L. Sabharwal and J. L. Leopold, "Cardinal direction relations in qualitative spatial reasoning," *International Journal of Computer Science & Information Technology (IJCSIT)*, vol. 6, no. 1, pp. 1–13, 2014.

[3] L. Ma, H. Li, S. Lian et al., "Expression and application of geospatial relation ontology," in *Proceedings of the International Conference on Geo informatics*, pp. 1–5, IEEE, 2013.

[4] W. Liu, X. Zhang, S. Li, and M. Ying, "Reasoning about cardinal directions between extended objects," *Artificial Intelligence*, vol. 174, no. 12-13, pp. 951–983, 2010.

[5] T. Chen and M. Schneider, "Modeling cardinal directions in the 3D space with the objects interaction cube matrix," in *Proceedings of the 25th Annual ACM Symposium on Applied Computing, SAC 2010*, pp. 906–910, March 2010.

[6] M. Wang and S. Li, "Research progress on formal description of spatial directional relations," *Computer Application*, vol. 33, no. 5, pp. 1324–1329, 2013.

[7] W. Gu and Y. Liu, "Description and reasoning of object-orientation-based direction relation in three-dimensional space," *Journal of Computational Information Systems*, vol. 7, no. 12, pp. 4433–4440, 2011.

[8] X. H. Song and D. T. Ouyang, "A qualitative spatial relation model for common sense spatial information processing," *Journal of Software*, vol. 23, no. 9, pp. 2311–2322, 2012.

[9] S. J. Li, "Combining topological and directional information for spatial reasoning," in *Proc. of the IJCAI*, M. M. Veloso, Ed., pp. 435–440, Hyderabad, India, 2007.

[10] N. Salamat and E. H. Zahzah, "Spatio-temporal reasoning by combined topological and directional relations information," *International Journal of Artificial Intelligence & Soft Computing*, vol. 3, no. 2, pp. 185–201, 2012.

[11] X. Liu, W. Liu, and C. Li, "Qualitative description and reasoning of topological relation in three-dimensional GIS," in *Proceedings of the 2008 3rd International Conference on Innovative Computing Information and Control*, pp. 115–121, June 2008.

[12] H. X. Hao, P. L. Zhang, and L. I. Songb, "3DR44 direction relation representation model in three dimensional space," *Computer Engineering*, vol. 37, no. 1, pp. 74–80, 2011.

[13] Z. H. Wang, H. W. Yan, Y. C. Yang et al., "Compound spatial query based on direction and distance relation," *Engineering of Surveying & Mapping*, vol. 23, no. 11, pp. 7–12, 2014.

[14] W. Sun, J. Ouyang, L. Huo et al., "Modeling direction relations between uncertain regions," *Journal of Computational Information Systems*, vol. 8, no. 19, pp. 25–43, 2012.

[15] R. K. Goyal and M. J. Egenhofer, "Similarity of cardinal directions," in *Proceedings of the International Symposium on Spatial and Temporal Databases*, pp. 36–58, Springer, 2001.